Recent progress in nanostructured electrodes for solid oxide fuel cells deposited by spray pyrolysis

Lucía dos Santos-Gómez[1,*], Javier Zamudio-García[2], José M. Porras-Vázquez[2], Enrique R. Losilla[2], David Marrero-López[3,*]

[1] Department of Physical and Analytical Chemistry, Oviedo University-CINN-CSIC, 33006-Oviedo, Spain.

[2] Universidad de Málaga, Dpto. de Química Inorgánica, Cristalografía y Mineralogía, 29071-Málaga, Spain.

[3] Universidad de Málaga, Dpto. de Física Aplicada I, 29071-Málaga, Spain.

Keywords: spray-pyrolysis; SOFC; cathode; anode; nanomaterials; nanocomposites; active layers

Abstract

Low-temperature solid oxide fuel cells (LT-SOFCs), operating below 650 ºC, are attracting a great interest due to their long-term stability and potential application for stationary and portable power generation. Much effort is being devoted to investigating new electrode materials because the electrode polarization resistance remains a serious limitation to the performance. Nanostructured electrodes offer the possibility of increasing the SOFC efficiency at low temperatures. Among the different electrode preparation techniques, spray pyrolysis deposition is a versatile, economic and industrially scalable method to grow electrodes directly on the electrolyte, reducing preparation steps and time. Recent progresses in this field are summarized here, especially highlighting the wide variety of different microstructural strategies used to improve the electrode performance, i.e. nanocomposite cathodes graded cathodes, infiltrated cathodes and cathodes with active/functional layers. Finally, the current existing challenges and the future working directions for further enhancing the properties of new nanostructured electrodes are discussed.

* Corresponding author.
E-mail address: marrero@uma.es (David Marrero-López); ldsg@uniovi.es (Lucía dos Santos-Gómez)
Present address: Dpto. de Física Aplicada I, Facultad de Ciencias, Campus de Teatinos, Universidad de Málaga, 29071-Málaga, Spain.
Tel: +34 952137057, Fax: +34 952132382

Contents

1. Introduction

Nowadays, above 80% of the global energy consumption comes from the combustion of fossil fuels with the consequent increase of CO_2 emissions [1,2]. Thus, the development of environmentally friendly, cost effective and highly-efficient energy conversion and storage devices is desirable to mitigate the global warming. In this context, fuel cells are reversible electrochemical devices that can operate under both fuel cell mode for electrical energy generation, and electrolysis mode for hydrogen production using electricity from renewable sources [3,4].

Proton exchange membrane fuel cells (PEMFCs) are the most developed technology due to their low operating temperature, typically below 100 ºC. However, these cells exhibit several drawbacks, including high cost of the Pt-based electrocatalysts and susceptibility to poisoning by nitrogen and sulphur containing species [5,6]. In contrast, the high operating temperatures of Solid Oxide Fuel Cells (SOFCs) offer the opportunity of using not only hydrogen but also hydrocarbon-based fuels [7-10].

A typical SOFC is comprised by three main ceramic components: electrolyte, cathode and anode. The electrolyte is a pure ionic conductor (O^{2-}, H^{+}), while the anode and cathode are mixed ionic-electronic conductors. Traditionally, yttria-stabilized zirconia, $Zr_{0.84}Y_{0.16}O_{1.92}$ (YSZ), has been the most employed electrolyte due to its high temperature phase stability for operation at 800-1000 ºC. Unfortunately, the oxide ion conductivity at low temperature (6 mS cm^{-1} at 650 ºC) is too low for practical applications. Another issue is the reaction of YSZ with high efficiency mixed ionic electronic conductors (MIEC), developed in the last few years, based on cobalt and iron containing perovskites, i.e. $(La,Sr)(Co,Fe)O_{3-\delta}$ (LSCF), $(Ba,Sr)(Co,Fe)O_{3-\delta}$ (BSCF) and $(Pr,Ba,Sr)(Co,Fe,Mn)O_{6-\delta}$ [11-17]. This is the main reason why $(La,Sr)MnO_3$-based materials (LSM) are still considered to be the most appropriate cathode for SOFCs, despite their poor efficiency at intermediate temperatures (600-800 ºC).

Electrolytes based on $Ce_{1-x}A_xO_{2-\delta}$ (A=Gd and Sm, $x \leq 0.2$) are considered the most suitable for low temperature solid oxide fuel cells (LT-SOFCs) applications due to their high ionic conductivity (20 mS cm^{-1} at 650 ºC). In addition, they are chemically compatible with most of the cathode materials [18]. $La_{0.8}Sr_{0.2}Ga_{0.8}Mg_{0.2}O_{3-\delta}$ (LSGM) also exhibits high values of ionic conductivity (33 mS cm^{-1} at 650 ºC) in the intermediate temperature range (600-800 ºC), but it is difficult to synthesize and the high cost of gallium hinders its application [19,20].

The anode material is usually a Ni-based cermet, i.e. Ni-YSZ and Ni-CGO, with high electronic conductivity and good electrocatalytic activity towards fuel oxidation; however, they exhibit several drawbacks when fueled with hydrocarbons, such as carbon and sulfur deposition. Alternative anode materials based on perovskite-type structures have also been investigated, including $La_{0.8}Sr_{0.2}Cr_{0.5}Mn_{0.5}O_{3-\delta}$, doped- $SrTiO_{3-\delta}$, $SrFeO_{3-\delta}$ and $Sr_2MgMoO_{6-\delta}$ [21-26].

In addition to the choice of suitable materials for SOFC construction, this technology is still hindered by several issues regarding the performance, durability and fabrication costs of the cells [27]. In particular, the operating temperature of SOFCs is too high for their practical implementation; therefore, lowering the operating temperature to the range of 400-600 ºC is one of the main goals to improve the life time of the cell and promote their commercialization. However, fuel cell performance is reduced at low operating temperature due to the poorer ionic conductivity of the electrolyte, as well as the low electrocatalytic activity of the electrodes towards both fuel oxidation and oxygen reduction reaction (ORR) [28].

On the other hand, the manufacturing processes of SOFCs play an important role on the SOFC performance. In particular, the cell assembly needs to be carried out without causing any performance degradation of the cell components due to their reactivity and minimizing the engineering costs. The planar and tubular SOFC configurations, typically supported on the anode material, are usually prepared via tape-casting and extrusion moulding, respectively [29,30]. Both anode and electrolyte, Ni-YSZ/YSZ or Ni-CGO/CGO, are simultaneously sintered at elevated temperatures and then the cathode is deposited by chemical or physical techniques [31]. The main advantage of these SOFC configurations is that the cathode is fixed in the last stage at a lower temperature, avoiding possible reactions with the electrolyte and coarsening of the microstructure. Different studies have demonstrated that the electrode performance strongly depends on the microstructure [32-35]. Electrodes with a low specific surface area have limited active sites for the electrochemical reactions and, consequently, a poor efficiency. In contrast, electrodes with a large surface area, i.e. an extended triple phase boundary (TPB) length, are more efficient because of the numerous interfacial active sites available for the electrochemical processes. Among the different strategies used to extend the TPB, the development of nanostructured electrodes with high activity, appropriate porosity and robust stability has attracted special interest in the last few years [36-42].

For industrial applications, the electrode preparation should be simple, involving as few steps as possible to reduce fabrication costs and time. In this context, the traditional solid-state reaction method includes several firing and grinding processes of the raw materials, resulting in powders with relatively large grain size and low active areas. In recent years, numerous synthetic strategies have been developed to fabricate nanostructured electrodes, such as sol-gel [43], freeze-drying [44], electrospinning [45,46], template method [47,48], microwave combustion [49], hydrothermal techniques [50,51] and infiltration [52-54]. Most of these synthetic methods lead to the formation of single-phase materials with fine particle size and high electrocatalytic activity. However, they are usually employed at laboratory scale for the design and construction of nanostructured electrochemical devices, generally requiring strict synthetic conditions, long reaction times and tedious procedures, which limit their applicability at industrial level. Moreover, multiple processing steps are still required

in order to adhere these electrodes to the electrolyte, including: (i) preparation of an ink containing organic additives, i.e. binders and pore formers; (ii) deposition of the ink by screen-printing or dip-coating on the electrolyte; and (iii) sintering at rather high temperatures to ensure sufficient adhesion to the electrolyte. Such high sintering temperatures lead to a significant grain growth and low porosity, affecting negatively the electrochemical properties of the as-prepared materials. Hence, scalable, efficient, facile, economic and industrially viable processing and synthetic methods for the production of nanostructured electrodes are key to further commercialize the SOFC technology. The direct electrode preparation on the electrolyte at low temperatures would result in several benefits: i) the particle size is reduced and, consequently, the electrocatalytic activity is enhanced; and ii) the adherence and integrity of the electrodes to the substrate, based on chemical bonding, are improved compared to ink-based depositions.

Among the different deposition techniques (e.g. spin and dip-coating, chemical vapor deposition, pulsed laser deposition and magnetron-sputtering), spray pyrolysis has demonstrated to be an economical approach to prepare nanostructured electrodes with different architectures, offering the following advantages over the conventional methods: (i) simple, automatable and industrially scalable process; (ii) preparation of layers in a single deposition step, reducing time and fabrication costs; and (iii) highly reproducible process over large areas [55]. Although it was initially proposed to create dense thin films, highly porous layers can be also produced by tailoring the deposition conditions, being possible to control the quality and thickness of the layers, depending on the desired application.

Bearing in mind all these aspects, this review summarizes novel strategies to prepare highly efficient electrodes for SOFCs by spray-pyrolysis deposition. Firstly, a brief description of the most employed spray-based techniques in SOFC technology is presented. Secondly, the different microstructural strategies used to improve the cathode performance in the last few years, are discussed, including single phase cathodes, nanocomposite cathodes, infiltrated cathodes, and cathode with active/protective layers. Thirdly, anode materials prepared by spray-pyrolysis are addressed. Finally, conclusions and future perspectives on the development and application of nanostructured electrodes for LT-SOFCs are presented.

2. Electrode preparation techniques based on spray deposition

Spray deposition is a versatile technique widely used for the preparation of thin films and powder nanoparticles with different compositions, including metals, oxides and sulfides, among others [56,57]. Nanostructured materials, which are difficult to obtain by other techniques, can be prepared by spray deposition since their structure is determined by the formation of a metastable phase, prevailing over thermodynamic aspects [55]. In contrast to other preparation techniques, such as chemical vapor deposition, the stoichiometry of the initial precursor solution is maintained in the resulting film. Among the spray-based techniques, the most commonly employed in SOFC technology are conventional spray-pyrolysis deposition (CSD), ultrasonic-spray-pyrolysis deposition (USD), electrostatic-spray deposition (ESD) and flame-spray deposition (FSD). Each of them is briefly described below.

2.1. Conventional spray pyrolysis deposition (CSD)

Conventional spray pyrolysis deposition is a direct preparation method performed with cheap and affordable equipment, making it a perfect option for industrial implementation [58,59]. The usual setup includes: (i) a nozzle to atomize the precursor solution into fine drops by using compressed air, (ii) a syringe pump to continuously deliver the precursor solution at a defined flow rate; and (iii) a metal heated block with a thermocouple to control the substrate temperature (Fig. 1a).

A diluted precursor solution, containing stoichiometric amounts of the appropriate metallic salts, is pumped, atomized, and sprayed onto a heated substrate. The solution atomization is a critical step since it controls the size and distribution of the drops. This process is carried out by forcing the solution to pass through a small aperture of the nozzle, forming small drops with high speed. Generally, the most frequently used nozzles are those in which the atomization is produced by the Venturi effect. After the atomization stage, the sprayed drops reach the hot substrate, evaporating the solvent and thermally decomposing the precursors, creating a thin film of the desired material. Unlike physical deposition techniques, CSD deposition does not require the use of high purity targets or expensive crystallographically oriented substrates. Moreover, vacuum pumps are not needed at any stage of the process, offering enormous benefits for industrial implementation.

The starting precursor salts are usually metal nitrates, acetates and oxalates, which decompose easily at low temperature without leaving residues on the film. Moreover, these salts are usually solved in water, reducing costs and toxicity problems. The film morphology and thickness are tailored by modifying the experimental conditions, such as nozzle to substrate distance, deposition temperature, time, precursor type and air flow rate [59].

2.2. Ultrasonic spray-pyrolysis deposition (USD)

Ultrasonic spray deposition is a variant of the spray-pyrolysis technique based on an aerosol process. The principal difference compared to CSD consists in the use of an ultrasonic nebulizer, and alternatively, an ultrasonic spray-nozzle, which vibrates at high frequencies (Fig. 1b). In this approach, only Newtonian fluids with low viscosity can pass through the vibrating zone, where the fluid is broken into fine droplets, creating an aerosol, which is transported by a gas carrier to the heated substrate to form the film. USD has the advantage of uniform atomization of particles, operates at extremely low air pressure and is suitable for small-area coatings in contrast to CSD. This technique has been employed to obtain hollow, solid spheres and thin film materials with a wide variety of applications in solar cells, gas sensors and SOFCs [59,60]. The advantages and disadvantages of the different spray-pyrolysis techniques are summarized in Table 1.

2.3. Electrostatic spray pyrolysis deposition (ESD)

In this technique, the solution atomization is carried out by applying a high voltage between the nozzle and the hot substrate, generating electrohydrodynamic forces that atomize the precursor solution (Fig. 1c). The electrostatic atomization process mainly consists of two parts: the extractor electrode and the nozzle. The electrode is earthed and the nozzle is supplied with a high DC voltage (2-15 kV) or vice versa. The charged droplets are transported thanks to the electrical field, impacting on the hot substrate and forming the film.

Both the electrical field and the spreading of the droplets are important parameters that influence the final microstructure of the films. The drop size distribution is strongly dependent on the surface tension, concentration, and the conductivity of the precursor solution, according to the Ganan-Calvo model [61-64]. The main advantage of this technique is the smaller size of the droplets compared to those obtained by other atomization techniques. Furthermore, the electrical repulsions of the charged droplets prevent their agglomeration leading to a uniform size distribution.

Similarly to other spray-pyrolysis-based techniques, the substrate temperature is one of the main parameters to control the films microstructure, and consequently, their properties [65]. Dense or porous morphologies may be obtained depending on the deposition conditions [66]. At relatively low temperatures and high flow rates, large drops with an excess of liquid impact on the substrate surface, creating cracked films due to the rapid evaporation of the solvent. In contrast, when the substrate temperature increases, the impacting droplets contain less solvent and hence denser films are obtained. Moreover, a very small variation in the temperature, such as 5 ºC, is enough to change the average size distribution of the droplets, and consequently, modify the microstructure of the layers [67]. Hence,

parameters, such as nozzle-substrate distance, temperature, time, solution conductivity, surface tension, boiling point and viscosity, need to be carefully controlled in ESD.

2.4. Flame spray pyrolysis deposition (FSD)

Flame spray deposition is a combination of flame synthesis and spray pyrolysis techniques, where an aqueous solution is sprayed through a capillary and into a flame (Fig. 1d) [68,69]. The flame, generated by igniting a mixture of CH_4 and O_2, supplies the required energy for the decomposition of the precursor drops. The main limitation of this technique is the poor mechanical stability of the deposited films as a consequence of the lower chemical bonding of the dried nanoparticles to the substrate [70]. The dispersion gas flow may be high enough to ensure an adequate residence time of the drops into the flame, limiting the solvent evaporation rate [71]. Hence, dense and porous microstructures for SOFC applications can be obtained by carefully controlling the experimental conditions, i.e. the precursor concentration, residence time, deposition temperature and the post-thermal treatment [72].

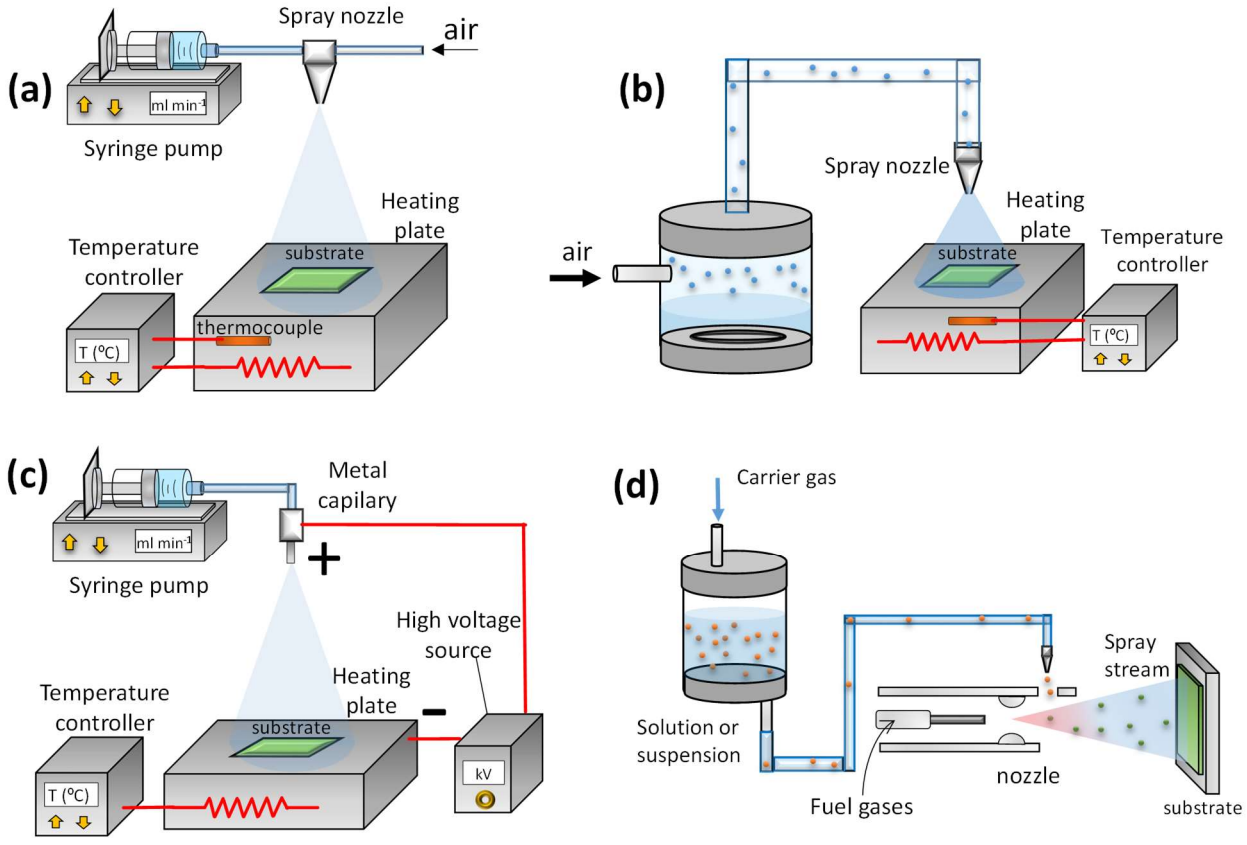

Fig. 1. Schematic representation of the different spray-pyrolysis techniques: (a) conventional spray-pyrolysis deposition (CSD), (b) ultrasonic spray-pyrolysis deposition (USD), (c) electrostatic spray deposition (ESD) and (d) flame spray pyrolysis deposition (FSD).

Table 1. Advantages and disadvantages of the different spray-pyrolysis deposition techniques.

Technique	Advantages	Disadvantages
Conventional spray pyrolysis deposition (CSD)	Simple and inexpensive equipment. Operates at atmospheric pressure (non-vacuum). Capability for large scale production. Low sensitivity to the precursors and solvents.	High air pressure for atomization and high flow rate. Variation of the Substrate temperature due to the high air flow rate.
Ultrasonic spray pyrolysis deposition (USD)	Low deposition temperature. Suitable for small area coating.	Only Newtonian fluids with low viscosity can be used.
Electrostatic spray pyrolysis deposition (ESD)	Smaller diameter of the precursor drops. No agglomeration of particles. Highly porous layers can be obtained.	High DC voltage. Carefully control of the solution conductivity, viscosity, surface tension and boiling point. Small variation of the substrate temperature modifies the microstructure of the layer.
Flame spray pyrolysis deposition (FSD)	High film growth rate. Precise control of the microstructure. Crystalline phases are obtained without additional annealing.	A flame is required. Carefully control of solvent boiling point and flow of dispersion gas. Low mechanical adherence of the coating.

3. Microstructural strategies for SOFC cathodes

Since the cathode plays a major role in determining the efficiency of LT-SOFCs, it is of great importance to improve its performance. In this section, different microstructural strategies used to improve the performance of cathode materials are discussed.

The main function of the cathode is to provide electrocatalytic active sites for the oxygen reduction reaction (ORR). The oxygen reduction is comprised by multiple steps that take place in the bulk and on the electrode surface. The cathode must possess a high porosity to facilitate the diffusion of the oxygen gas to the active sites for ORR. Moreover, high ionic and electronic conductivities are necessary to minimize the ohmic losses and favour the transport of oxide ions through the electrode/electrolyte interface [28,73].

Among the several processes involved in the ORR: gas diffusion, surface exchange (oxygen adsorption, dissociation and charge transfer), ion diffusion and charge transfer across the electrolyte/electrode interface, among others; the main limiting steps are the ion diffusion and the oxygen surface exchange [74,75]. The most outstanding cathodes to operate at intermediate temperatures are those known as mixed ionic-electronic conductors (MIECs), which possess high oxygen surface exchange coefficients (k) and elevated oxygen bulk diffusion coefficients (D_δ) [76-78]: $La_{0.6}Sr_{0.4}Co_{0.8}Fe_{0.2}O_{3-\delta}$ ($k=5.37\cdot10^{-6}$ cm·s^{-1} and $D=1.86\cdot10^{-8}$ cm^2·s^{-1} at 800 ºC [79]), $Ba_{0.5}Sr_{0.5}Co_{0.8}Fe_{0.2}O_{3-\delta}$ ($k=4.1\cdot10^{-3}$ cm·s^{-1} and D: $3.9\cdot10^{-4}$ cm^2·s^{-1} at 800 ºC [80]), $Sm_{0.5}Sr_{0.5}CoO_{3-\delta}$ and $PrBaCo_2O_{5+\delta}$ [81]

Regarding the performance of the electrodes, it is not only dependent on the crystal structure and chemical composition but also on the ceramic microstructure, since the electrochemical reactions

involve the ionic/electronic conductivity and surface properties. In order to improve the electrode performance, different microstructural strategies have been proposed in the literature. In cathodes with low ionic conductivity, such as LSM, the actives sites for the ORR are restricted to the triple phase boundary (TPB) region, near the electrolyte/electrode interface, and consequently, the efficiency is relatively poor (Fig. 2a). In this case, the addition of a second phase with high ionic conductivity, i.e. doped-CeO_2 and Bi_2O_3, to obtain a composite cathode, is one of the main strategies to enlarge the TPB (Fig. 2b) [82,83]. In contrast, in mixed ceramic conductors, such as LSCF and BSCF, the TPB is extended to the whole electrode surface and the cathodic efficiency is improved when compared to composite cathodes (Fig. 2c) [11-17]. Nevertheless, the performance is still limited by the large grain size of the electrodes prepared by conventional synthetic methods.

Since the interfaces are critical regions determining the efficiency and lifetime of the SOFCs, the introduction of active or protective layers between the cathode and the electrolyte is an alternative strategy to enhance the properties of the electrodes and durability of the cells (Fig. 2d) [84-86]. Surface modification of the electrodes via decoration with active nanoparticles, e.g. Pt and Pr_2O_6 or exsolved electrocatalytic nanoparticles [87-91], e.g. Ni, Co or Fe, are alternative strategies to improve the electrode efficiency (Fig. 2e). Another promising approach is the infiltration of a MIEC into a porous electrolyte backbone layer to increase the surface contact between an ionic and a mixed conductor, resulting in an increase of the electrochemically active sites [38,52-54] (Fig. 2f). Finally, nanostructured electrodes, formed by a single (Fig. 2g) or a composite electrode (Fig. 2h), exhibit better properties than those produced by conventional synthetic methods due to the increased surface area and TPB density [40,41].

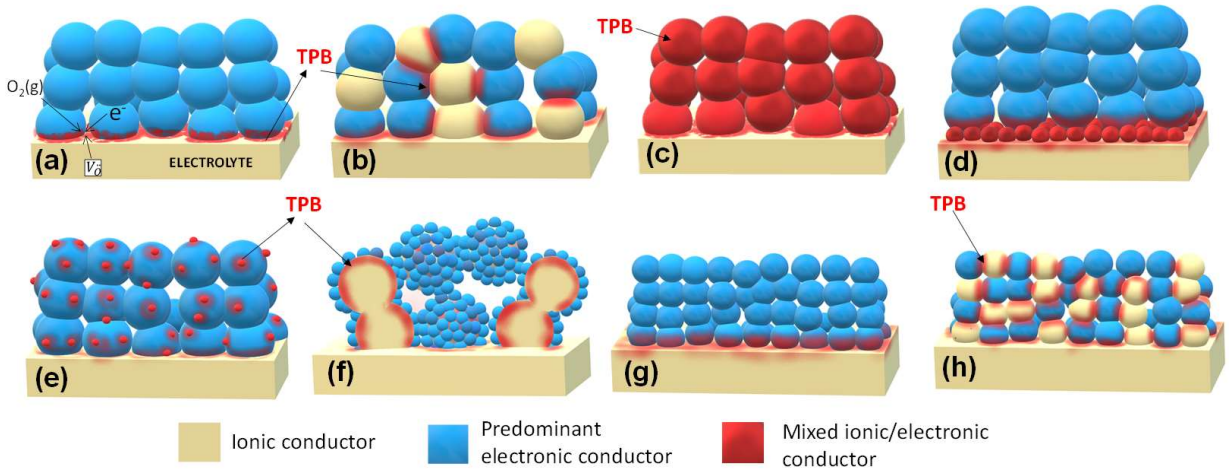

Fig. 2. Representation of different microstructural strategies used to improve the performance of SOFC electrodes: (a) a poor ionic conductor with limited TPB at the electrode/electrolyte interface, (b) a composite electrode, (c) a mixed conductor with extended TPB on the whole surface, (d) an active layer introduced between the electrode and the electrolyte, (e) an electrode decorated with active nanoparticles, (f) an infiltrated electrode into a porous backbone layer, (g) a nanostructured electrode and (h) a nanocomposite electrode.

3.1. Single-phase cathodes

In recent years, cathodes based on single perovskite oxides, e.g. $La_{0.8}Sr_{0.2}MnO_{3-\delta}$ (LSM), $La_{0.6}Sr_{0.4}Co_{1-x}Fe_xO_{3-\delta}$ (LSCFx), $Sm_{0.5}Sr_{0.5}O_{3-\delta}$ (SSC) and layered perovskites, e.g. $PrBaCo_2O_{5+\delta}$ and La_2NiO_4, have been prepared by spray-pyrolysis deposition. In general, the electrode properties have been improved by lowering the deposition temperature in order to obtain nanostructured electrodes. Different morphologies and properties have been obtained, depending on the technique used and the preparation conditions, which are summarized below.

$La_{0.8}Sr_{0.2}MnO_{3-\delta}$ (LSM) based cathodes

The traditional LSM cathode, which is only considered for SOFC applications at temperatures higher than 800 ºC, has been prepared by different spray-pyrolysis routes in order to improve its electrochemical properties at low temperature. The first studies were mainly focused on the preparation, crystal structure and morphology of LSM layers, paying little attention to their electrochemical properties for SOFC applications. In 2004, Princivalle *et al*. deposited LSM films on YSZ by electrostatic spray pyrolysis (ESD) [92]. Films with different superficial morphologies, i.e. porous, cracked and dense, were obtained by varying the precursor salt type, flow rate and deposition temperature. In general, cracked layers were obtained below 250 ºC, porous layers at 300 ºC and dense layers above this temperature.

The effects of the type of precursor and solvent on the compositional homogeneity and morphology of the LSM films were also investigated by Hademani *et al.* [93]. Ultrasonic spray deposition (USD) was used to obtain porous LSM cathodes on YSZ electrolytes. The films prepared from organo-metallic precursors and organic solvents showed a homogeneous crack-free morphology, contrary to those obtained from aqueous solutions. Highly porous layers were obtained by increasing the temperature and solution flow rate [93]. Later, ESD was also used to obtain nanoporous LSM films on YSZ at 900 ºC, a temperature significantly lower than that used in conventional methods [94]. The common reaction products between YSZ and LSM, i.e. $La_2Zr_2O_7$ and $SrZrO_3$, were not found. The polarization resistance decreased from 15 to 1.2 Ω cm^2 in the temperature range of 546-777 °C.

Marrero-López *et al.* prepared LSM layers by CSD on YSZ electrolytes at 250 ºC from an aqueous solution of metal nitrates. The influence of the post-annealing temperature (650-1100 ºC) on the microstructure and electrical properties was investigated [95]. Porous layers with an average particle size of 50 nm were obtained at temperatures lower than 850 ºC. The values of polarization resistance were as low as 1.8 Ω cm^2 at 600 ºC compared to 27.2 Ω cm^2 for a commercial screen-printed LSM cathode. The layers annealed at temperatures above 850 ºC suffered a drastic reduction of the porosity and the grain size grew up to 240 nm at 1050 ºC. As a consequence, the polarization resistance increased from 1.8 to 15.8 Ω cm^2 at 600 ºC; however, these values were still lower than those obtained

for screen-printed cathodes. These results confirmed that the efficiency of the LSM layers, prepared by spray-based techniques, is closely related to the annealing temperature and microstructure. Thus, these cathodes have potential application in LT-SOFCs.

$La_{0.6}Sr_{0.4}Co_{1-x}Fe_xO_{3-\delta}$ based cathodes

The $La_{0.6}Sr_{0.4}Co_{1-x}Fe_xO_{3-\delta}$ (LSCF) cathode has been prepared with different morphologies by ESD. For example, Marinha *et al.* deposited LSCF films onto a CGO electrolyte with dense, cracked and coral-like architectures, by changing the deposition temperature (250-450 °C), the nozzle-substrate distance (15-45 mm) and the precursor flow rate (0.34-1.5 mL h^{-1}) (Fig. 3a-3c) [96,97]. The polarization resistance varied between 0.82 and 6.23 Ω cm^2 at 600 ºC, with the lowest values for those samples with larger surface areas. The electrode polarization contribution associated with the oxygen exchange was the dominant limiting factor for ORR, further confirming the importance of the morphology on the cathode efficiency [97]. In a subsequent study, cracked and coral-like LSCF films were coated with a screen-printed LSCF current collector layer and investigated by impedance spectroscopy [98]. The introduction of the current collection layer reduced the polarization resistance from 0.82 to 0.13 Ω cm^2 at 600 ºC. Moreover, the coral-like films demonstrated an improved durability, and a stable polarization resistance at 600 ºC for 130 h compared to the cracked films.

The influence of the solvent type on the morphology of LSCF cathodes prepared by ESD was investigated by Sindiraç *et al.* [99]. The results revealed that a mixture of 2-butoxyethanol and ethylene-glycol should be employed instead of the conventional solvents used in the literature (ethanol and buty-carbitol) with lower boiling point. The deposition temperature was optimized at 350 ºC, achieving the coral-like and the cracked films R_p values of 0.82 and 1.63 Ω cm^2 at 700 ºC, respectively [99].

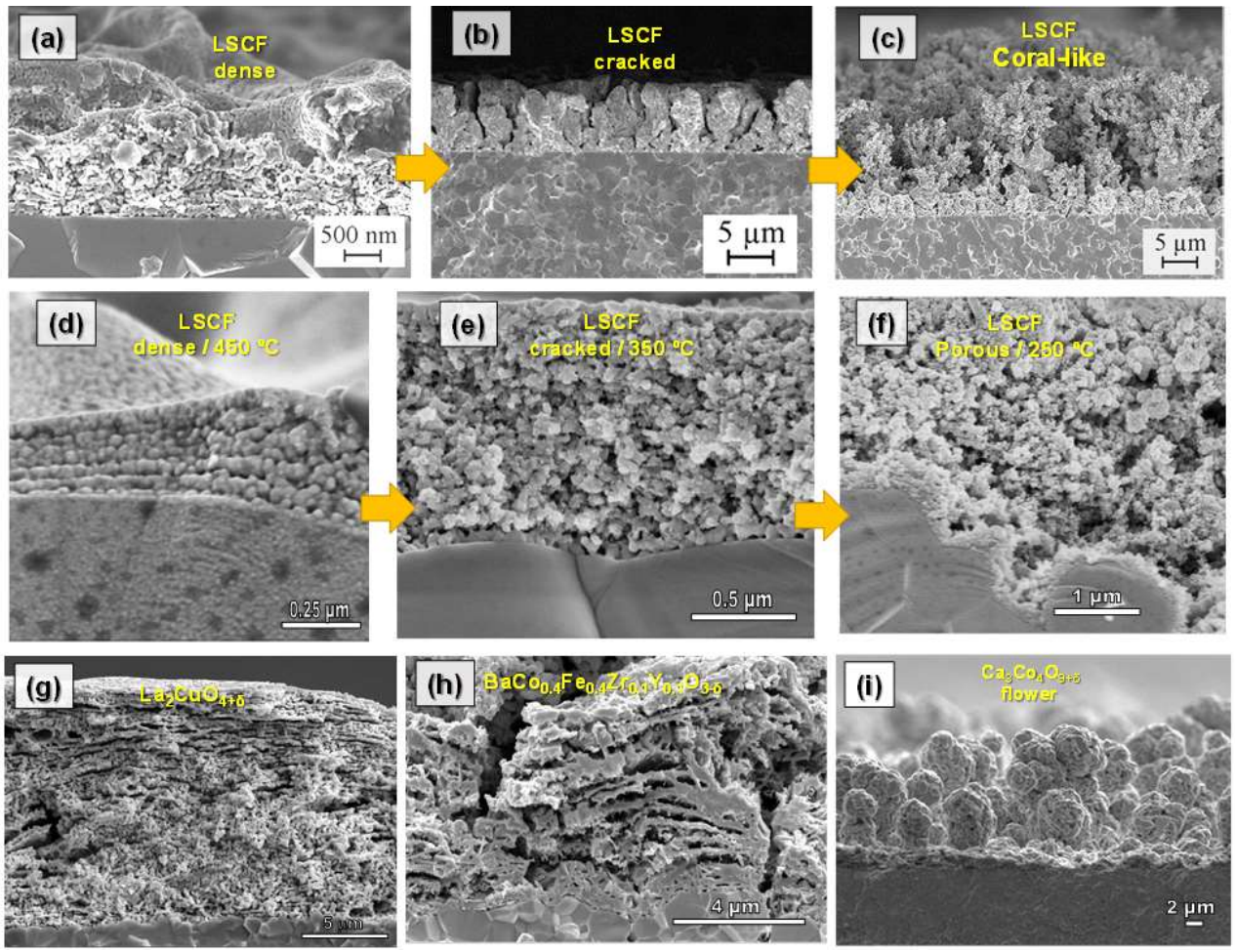

Fig. 3. SEM images of several cathode materials with different morphologies obtained by spray-pyrolysis deposition techniques: (a-c) $La_{0.6}Sr_{0.4}Co_{0.8}Fe_{0.2}O_{3-\delta}$ by ESD [97], Copyright 2011 American Chemical Society; (d-f) $La_{0.6}Sr_{0.4}Co_{0.8}Fe_{0.2}O_{3-\delta}$ by CSD [100], Copyright 2014 Elsevier; (g) $La_2CuO_{4-\delta}$ by CSD [105], Copyright 2019 Elsevier; (h) $BaCo_{0.4}Fe_{0.4}Zr_{0.1}Y_{0.1}O_{3-\delta}$ by CSD [110], Copyright 2020 MDPI; and (i) $Ca_3Co_4O_{9+\delta}$ by ESD [112], Copyright 2016 Elsevier

By considering the low thermal stability of the nanostructured electrodes, the effects of the deposition and annealing temperature on the microstructural and electrical properties of LSCF films were investigated [100]. LSCF films were deposited onto CGO electrolytes by CSD at different temperatures between 250 and 450 ºC, obtaining electrodes with different morphologies and porosities, i.e. dense, cracked and porous (Fig. 3d-3f). A clear relationship was found between the starting porosity of the electrodes, the annealing temperature and the polarization resistance. Dense LSCF films deposited at 450 ºC exhibited a significant increase of the polarization resistance from 0.12 to 1.1 Ω cm^2 at 600 ºC after increasing the annealing temperature from 650 to 850 ºC. This was attributed to an increase of the particle size, from 30 to 78 nm, and the concomitant reduction of the TPB density. In contrast, the porous layers deposited at 250 ºC exhibited a lower variation of the particle size with the annealing temperature, from 55 to 61 nm at 650 and 850 ºC, respectively, and hence, only a slight increase of the polarization resistance was detected, from 0.16 to 0.24 Ω cm^2 at 600 ºC [100]. The

authors concluded that highly porous LSCF cathodes exhibit sufficient microstructural stability for application in LT-SOFCs.

Although LSCF and YSZ are chemically incompatible at high sintering temperatures, Prakash *et al.* deposited LSCF layers on YSZ by plasma spraying [101]. No evidence of reaction was observed at the interface of both materials due to the low sintering temperature used, 800 ºC. A durability test was performed at 750 ºC for 100 h and no changes in the polarization resistance were detected. This study confirmed that LSCF could be directly deposited on YSZ without any protective interlayer, such as CGO, providing that the operation and fabrication temperature are lower than 800 ºC.

In order to tailor the microstructure of LSCF cathodes, Wang *et al.* have proposed an alternative procedure based on Atmospheric Laminar Plasma Spray [102]. The LSCF films showed lower particle size and numerous vertical channels that facilitate the oxygen diffusion inside the electrode, obtaining R_p values of 0.31 Ω cm^2 at 750 ºC. A cell with Sc-stabilized zirconia electrolyte (ScSZ), NiO-ScSZ/ScSZ/LSCF, was deposited on stainless steel substrates by plasma spraying and generated a power density of 1.5 W cm^{-2} at 750 ºC. Another interesting strategy to obtain LSCF cathodes, based on electrostatic slurry spray deposition, was proposed for the first time by Lee *et al.* [103]. By using the powder-ball generation phenomenon in the electrostatic slurry spray deposition, micro-sized CGO powder-balls were deposited onto a CGO electrolyte to expand the TPB length, followed by the deposition of LSCF. The resulting cathode showed a polarization resistance of 0.1 Ω cm^2 at 650 ºC and a maximum power density of 0.7 W cm^2 for NiO-CGO/CGO/LSCF cell at the same temperature.

In another study, dense $La_{0.6}Sr_{0.4}CoO_{3-\delta}$ (LSC) films were deposited by flame spray deposition (FSD) [68]. The as-prepared films at 200 ºC were dense and amorphous. Upon calcining between 700 and 800 ºC, the films developed between 10-23% of porosity due to outgassing of organic residues, and densified after further annealing treatments. A R_p value of 0.96 Ω cm^2 at 600 ºC was obtained for the films annealed at 600 ºC. Higher temperatures resulted in worse R_p values due to the loss of porosity and grain-coarsening.

Perovskite-related cathodes

Although most of the cathodes prepared by spray deposition techniques are focused on perovskite type structures derived from LSM and LSCF, electrodes with different crystal structures have been also reported. For instance, $La_{n+1}Ni_nO_{3n+1}$ (n=0, 1, 3) films have been prepared by CSD [104]. Different crystal structures were stabilized depending on the annealing treatment, in accordance with the phase diagram of this system. $LaNiO_{3-\delta}$ perovskite was obtained at annealing temperatures between 540 and 800 °C, while $La_4Ni_3O_{10-\delta}$, with a Ruddlesden–Popper (RP) type structure and better electrochemical

properties, was stabilized after calcining at 1100 °C. The films exhibited a high electrical conductivity (80 S cm^{-1}), between room temperature and 600 ºC, but the polarization resistance was rather high due to the dense microstructure, e.g. 200 Ω cm^2 at 600 ºC for $La_4Ni_3O_{10-\delta}$. The analogous lanthanum cuprates, $La_2CuO_{4+\delta}$, have been also prepared by CSD [105]. The required annealing temperature to obtain a single compound was only 750 ºC compared to 1000 ºC for lanthanum nickelates. Thick layers of approximately 15 μm thickness, 40% porosity and well-connected particles with a diameter of 220 nm were obtained (Fig. 3g). The values of polarization resistance were as low as 1 Ω cm^2 at 600 ºC, which was attributed to the optimized microstructural morphology of these electrodes, as well as the lower sintering temperature that suppressed the reactivity with YSZ electrolyte.

The layered perovskite $PrBaCo_2O_{5+\delta}$ (PBC) was prepared on $SrTiO_3$ substrates by CSD to determine the surface exchange coefficient (k_{chem}) by electrical conductivity relaxation measurements [106]. Later, dos Santos-Gómez *et al*. obtained PBC cathodes by the same technique on CGO electrolytes [107]. The nanostructured cathodes presented an average particle size of 50 nm after sintering at 950 ºC, which was much lower than those obtained by screen-printed cathodes prepared from freeze-dried precursors (300 nm). The R_p values were also significantly improved, i.e. 0.082 and 0.22 Ω cm^2 at 600 ºC for nanostructured and screen-printed electrodes, respectively. In another study, Zhang *et al*. studied the influence of Fe-doping in $PrBaCo_{2-x}Fe_xO_{5+\delta}$ (PBSCF), an A-site ordered perovskite structure prepared by plasma spraying [108]. The lowest polarization resistance was achieved for the composition with (x=0.4) with a value of 0.074 Ω cm^2 at 600 ºC. No degradation at 600 ºC after 300 h was observed for any of the studied cathodes. Moreover, a remarkable maximum power output of 1.35 W cm^{-2} at 700 °C was achieved. In 2019, a related composition, $PrBa_{0.5}Sr_{0.5}Co_{1.5}Fe_{0.5}O_{5+\delta}$ (PBSCF) ordered perovskite, was deposited by CSD and studied by density functional theory (DFT) and molecular dynamics (MD) for its implementation as cathode in a SOFC [109]. The dense films showed a thickness-dependent electrochemical performance that was attributed to bulk diffusion limitations. The estimated oxygen anion diffusion coefficient for the bulk PBSCF was of $D=2.98\cdot10^{-10}$ $cm^2\cdot s^{-1}$ and high values of R_p were found, 4 Ω cm^2 at 700 ºC. The authors concluded that the Ba-surface segregation plays a key role in reducing the oxide ion transport, limiting the electrochemical performance.

Other cathode compositions

In 2020, the novel $BaCo_{0.4}Fe_{0.4}Zr_{0.1}Y_{0.1}O_{3-\delta}$ (BCFZY) single perovskite cathode was deposited by CSD on a CGO electrolyte [110]. A laminated-type morphology with high porosity, particle size of 50 nm and good adherence to the CGO electrolyte was obtained (Fig. 3h). Very low R_p values were achieved for the nanostructured cathodes, i.e. 0.067 Ω cm^2 at 600 ºC, compared to 0.52 Ω cm^2 for a

screen-printed cathode with the same composition. A NiO-CGO/CGO anode supported cell with a nanostructured BCFZY cathode generated a power density of ~ 1 W cm^{-2} at 600 °C.

$Sm_{0.5}Sr_{0.5}CoO_{3-\delta}$ (SSC), was deposited by ESD on a CGO electrolyte, obtaining layers with a highly porous reticular structure. The electrodes exhibited a superior performance compared to that of a screen-printed cathode, 0.057 and 1.58 Ω cm^2, respectively at 650 ºC [111]. The ESD technique was also used to prepare $Ca_3Co_4O_{9+\delta}$ layers with a gypsum-flower-like morphology [112], but high values of R_p were obtained, 22.9 Ω cm^2 at 600 ºC (Fig. 3i).

Table 2. Electrode properties for single cathodes prepared by different spray-pyrolysis deposition techniques. Polarization resistance in air are given at 600 ºC. In those cases, where not data are available at 600 ºC, the temperature is included.

Cathode	Abbreviation	Technique	Thickness (µm)	Particle size (nm)	Electrolyte	R_p^{air} (Ω cm^2)	Ref.
$La_{0.8}Sr_{0.2}MnO_{3-\delta}$	LSM	ESD	2	--	YSZ	15 (546 ºC)	94
$La_{0.8}Sr_{0.2}MnO_{3-\delta}$	LSM	CSD	5	50	YSZ	1.8	95
$La_{0.6}Sr_{0.4}Co_{0.8}Fe_{0.2}O_{3-\delta}$	LSCF	ESD	--	--	CGO	6.23-0.82	97
$La_{0.6}Sr_{0.4}Co_{0.8}Fe_{0.2}O_{3-\delta}$	LSCF	ESD	7	--	CGO	0.82-0.13	98
$La_{0.6}Sr_{0.4}Co_{0.8}Fe_{0.2}O_{3-\delta}$	LSCF	ESD	20	--	CGO	7	99
$La_{0.6}Sr_{0.4}Co_{0.8}Fe_{0.2}O_{3-\delta}$	LSCF	CSD	--	55-61	CGO	0.16-0.24	100
$La_{0.6}Sr_{0.4}Co_{0.2}Fe_{0.8}O_{3-\delta}$	LSCF0.8	CSD	6	--	CGO	0.29	138
$La_{0.6}Sr_{0.4}CoO_{3-\delta}$	LSC	FSD	450	21-124	CGO	0.40 (650ºC)	68
$La_{0.6}Sr_{0.4}CoO_{3-\delta}$	LSC	ESD	--	80	YSZ/CGO	0.184 (650ºC)	174
$Ba_{0.25}La_{0.25}Sr_{0.5}Co_{0.8}Fe_{0.2}O_{3-\delta}$	BLSCF	CSD	--	35	CGO	0.30 (650ºC)	122
$Sm_{0.5}Sr_{0.5}CoO_{3-\delta}$	SSC	ESD	5	--	CGO	0.057 (650 ºC)	111
$PrBaCo_2O_{5+\delta}$	PBC	CSD	5	<50	CGO	0.082	107
$PrBaCo_{2-x}Fe_xO_{5+\delta}$	PBCF	FSD	20-25	--	ScSZ	0.074	108
$BaCo_{0.4}Fe_{0.4}Zr_{0.1}Y_{0.1}O_{3-\delta}$	BCFZY	CSD	7	30-90	CGO	0.17	110
$LaNiO_{3-\delta}$	LNO	CSD	0.35	50	CGO	200	104
$La_4Ni_3O_{10-\delta}$	--	CSD	0.35	350	CGO	500	104
$La_2NiO_{4+\delta}$	LNO	ESD	20	150	CGO	3.32	157
$La_2CuO_{4+\delta}$	LCO	ESD	15	220	CGO	1.00	105
$Pr_2NiO_{4+\delta}$	PNO	ESD	20	200	CGO	0.83	157
$LaPrNiO_{4+\delta}$	LPNO	ESD	27	130	CGO	0.72	157
$LaPrNiO_{4+\delta}$	LPNO	ESD	27	217	CGO	0.35 (700ºC)	158
$Ca_3Co_4O_{9+\delta}$	CCO	ESD	25-33	--	CGO	22.9	112

In general, single-phase cathodes, prepared by spray deposition at low temperature, exhibit lower polarization resistance compared to those obtained by the screen-printed method; however, their application is limited to the low temperature range (T<700 ºC) due to the low thermal stability of the nanostructured materials. Different approaches have been investigated to overcome this issue, which are discussed below. A summary of the electrochemical properties of several cathodes prepared by spray-pyrolysis are given in Table 2.

3.2. Nanostructured cathodes prepared from templates

The properties and performance of SOFC materials may be improved by using new procedures to control the microstructure and porosity [113-117]. In particular, the porosity of several materials for SOFC applications, e.g. LSM, LSCF, CGO, YSZ and Ni-YSZ, have been tailored by moulding methods [34,116-121]. Sacrificial templates, such as poly(methyl methacrylate) (PMMA), silica or carbon microspheres, have been employed because of their ability to create ordered porous materials when they are removed by thermal treatment. In these works, the as-prepared powders exhibited a regular porosity with high specific surface area, e.g. 38 m^2 g^{-1} for CGO and 25 m^2 g^{-1} for LSM [37], due to the low fabrication temperature (600 ºC). However, for SOFC applications, the powders need to be sintered at higher temperatures to ensure a good adhesion to the electrolyte, which usually results in a collapse of the macroscopic microstructure. In order to overcome this drawback, the combination of spray-pyrolysis and sacrificial templates has been proposed. By using CSD, Beckel *et al.* incorporated carbon black to the spray solution to obtain highly porous cathodes with better electrochemical efficiency [122]. In another study, LSM layers with tailored porosity were obtained by CSD by adding PMMA microspheres to an aqueous precursor solution [123]. The precursor solution was sprayed on YSZ substrates at low temperature (200 ºC) to prevent the decomposition of PMMA and then, the microspheres were eliminated during the post-deposition thermal treatment, obtaining layers with a regular pore size distribution of ~300 nm. These macroporous cathodes did not achieve improved electrochemical properties, compared to the same layers without pore formers; however, the stability after long-term operation was not investigated. It is worth noting that these highly porous cathodes should exhibit improved stability at high annealing temperatures as it was previously observed for single-phase cathodes.

3.3. Nanocomposite cathodes

It is reported that the efficiency of cathodes with poor ionic conductivity, such as LSM, may be improved by adding a second phase with high ionic conductivity, i.e. CeO_2 and Bi_2O_3-based electrolytes, to obtain a composite electrode. Many studies have shown that composite cathodes have higher efficiency than single-phase cathodes due to the increased TPB density (Fig. 2c) [82]. Moreover, they are usually employed to reduce the mechanical stress between the electrode and the electrolyte layers, originated by the different thermal expansion coefficients, enhancing the mechanical stability of the cell. Traditionally, composite cathodes are prepared by mixing the pristine materials but, unfortunately, it is difficult to control the composition distribution and architecture with this method.

In order to overcome this drawback, nanocomposite cathode powders are synthesized by different co-sintering methods. In particular, the nanocomposite electrode powders prepared by spray-pyrolysis showed a uniform distribution of nanosized crystals with high thermal stability and improved electrochemical properties. Different nanocomposite powders have been prepared, such as $Sm_{0.5}Sr_{0.5}CoO_{3-\delta}$-$Ce_{0.8}Sm_{0.2}O_{1.9}$ (SSC-CSO) [124], $Gd_{0.5}Sr_{0.5}CoO_{3-\delta}$-$Ce_{0.8}Gd_{0.2}O_{1.9}$ (GSC-CGO) [125] and $La_{0.4}Sr_{0.6}MnO_{3-\delta}$-$Ce_{0.8}Gd_{0.2}O_{1.9}$ (LSM-CGO) [126]. These nanocrystalline powders were deposited by screen-printing onto the electrolytes and sintered at relatively high temperatures (900-1200 ºC), achieving high power densities values, 3.13 W cm^{-2} at 750 ºC for SSC-CSO [124] and 1.66 W cm^{-2} at 700 ºC for GSC-CGO [125]. However, these results could be further improved by directly depositing the nanocomposite electrodes on the electrolyte to lower the sintering temperature and the particle size.

In 2008, Princivalle *et al.* reported the first nanocomposite film based on LSM-YSZ. The films were prepared by ESD with different YSZ contents, morphologies and porosities by varying the nozzle to substrate distance, the deposition temperature and nature of the precursor solution [127,128]. A precursor solution containing all the cations for both LSM and YSZ in stoichiometric amounts was employed without detecting any additional phase after calcination at 800 ºC. However, the electrochemical properties of these electrodes were not investigated. It is also worth noting that the same LSM-YSZ nanocomposite powders were prepared by spray-pyrolysis, followed by screen-printing deposition and sintering at 1200 ºC for 3 h, obtaining a porous cathode composed by particles of 100-200 nm in diameter [129]. A remarkable power density of 0.90 W cm^{-2} at 750 ºC was achieved in a Ni-YSZ/YSZ anode-supported SOFC.

LSM-CGO nanocomposite layers were also prepared by CSD [130]. The layers presented a reduced particle size of only 15 nm after sintering at 800 ºC, in comparison to 50 nm for the blank LSM cathode (Fig. 4a-4c). The fine particle size of the nanocomposite cathode was attributed to the presence of CGO as secondary phase, limiting the cation diffusion and the grain growth rate. In comparison, a screen-printed LSM-CGO cathode, obtained from a commercial mixture of nanostructured powders, showed a particle size 30 times larger after sintering at 1100 ºC. The polarization resistance of the spray-pyrolyzed cathode was as low as 0.29 Ω cm^2 at 600 °C, which was comparable to highly efficient cobaltite-based cathodes [12,13]. A single NiO-YSZ/YSZ anode supported cell with a LSM-CGO nanocomposite cathode generated a stable power density of 0.29 W cm^{-2} at 600 °C compared to 0.18 W cm^{-2} for the same cell with a conventional screen-printed cathode (Fig. 4d).

The $La_{0.6}Sr_{0.4}Co_{0.2}Fe_{0.8}O_{3-d}$-$Ce_{0.9}Gd_{0.1}O_{2-\delta}$ (LSCF-CGO) system has been further investigated in recent years. Angoua *et al*. prepared for the first time LSCF–CGO thin films by CSD from a single precursor solution [131]. The phase formation was investigated by XRD in the 500-900 ºC temperature range. Films calcined at 600 °C were a mixture of amorphous and crystalline particles with a diameter

lower than 5 nm. Above this temperature, the crystalline LSCF and CGO phases were formed. In a subsequent study, LSCF–CGO composite cathodes were deposited onto YSZ substrates by the same method [132]. The grain size of LSCF–CGO, with 41 wt.% CGO, ranged from 15 to 50 nm for annealing temperatures between 700 and 900 °C. The polarization resistance decreased with increasing CGO content from 30 Ω cm^2 for the blank LSCF to 3 Ω cm^2 for 60 wt.% LSCF-CGO at 600 ºC.

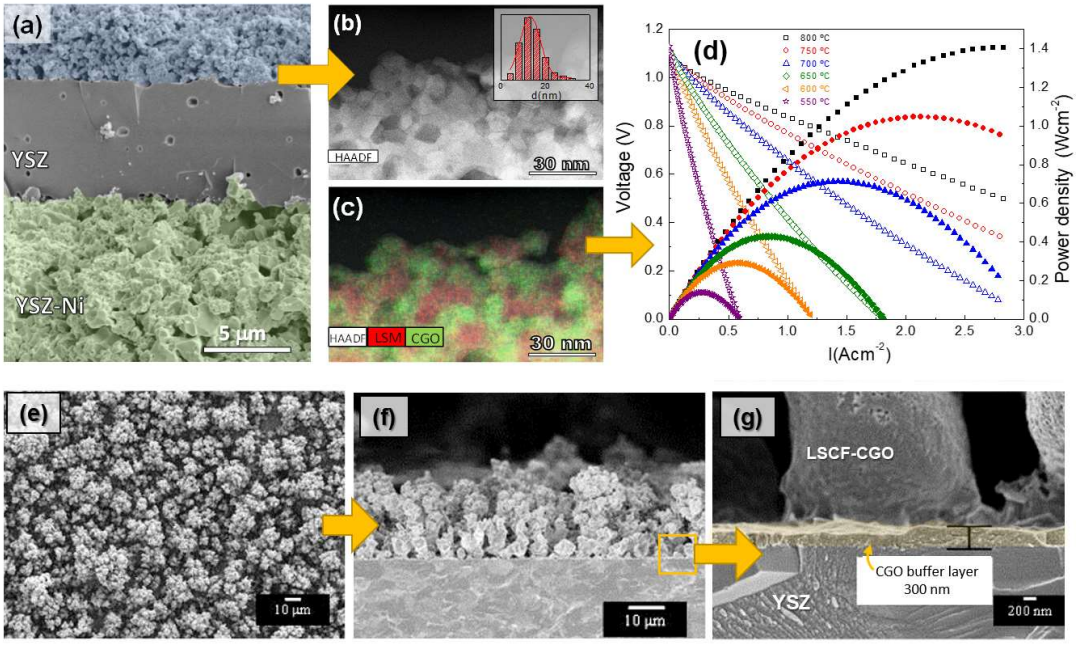

Fig. 4. (a) SEM image of a Ni-YSZ/YSZ anode supported cell with LSM-CGO nanocomposite cathode, (b,c) HAADF-STEM image and EDX of the nanocomposite cathode and the corresponding (d) voltage and power density curves [130], Copyright 2018 Elsevier. SEM images of a LSCF-CGO coral like microstructure: (e) surface view and (f-g) cross sectional views at different magnification [134], Copyright 2016 Elsevier.

By using ESD, Sar *et al.* prepared LSCF-CGO films with two different microstructures depending on the deposition temperature: a coral film at 350 ºC and a columnar film at 300 ºC [133,134]. Microstructural parameters such as open and closed porosity, specific surface area, percolation path and tortuosity factor were studied by X-ray nanotomography. A modelling approach with the 3D-Finite Element Method was used to assess the influence of the electrode microstructure and composition of LSCF-CGO on the electrochemical performance. The results estimated that the best performance is achieved for 20% of porosity and 60 vol.% CGO at 500 ºC in the LSCF-CGO composite, which agreed with the experimental results [135-137]. Later, the same authors prepared homogeneous and graded LSCF-CGO layers on YSZ with a thin and dense CGO buffer layer to avoid reactivity between LSCF and YSZ (Fig. 4e-f). Cells with and without LSCF screen-printed current collector layers were also investigated [134]. The lowest R_p values were obtained for cells with a current collector layer, i.e. 1.3 Ω cm^2 at 600 ºC, which was about 1.5 orders of magnitude lower than those without a current collector. Moreover, the polarization resistance was stable over time at 600 ºC.

More recently, dos Santos-Gómez *et al.* prepared LSCF-CGO nanocomposites with different LSCF-contents (50-100 wt.%) by CSD [138]. The particle size varied from 30 to 50 nm after sintering at 800 ºC and 1000 ºC, respectively. The polarization resistance decreased slightly with the addition of CGO, from 0.29 Ω cm^2 for the blank LSCF cathode to 0.16 Ω cm^2 for 50 wt.% LSCF-CGO at 600 ºC. A NiO-CGO/CGO anode supported cell with LSCF-CGO nanocomposite rendered a stable power density of 0.71 W cm^{-2} at 600 ºC compared to 0.39 W cm^{-2} for the same cell with a screen-printed cathode.

A recent report for the $La_{0.6}Sr_{0.4}Co_{0.8}Fe_{0.2}O_{3-\delta}$-CGO system revealed a decrease of the electrochemical activity with increasing CGO-content in comparison with the blank LSCF0.2 cathode, i.e. 0.72 Ω cm^2 for LSCF0.2 and 2.75 Ω cm^2 for LSCF0.2-40 wt.% CGO at 600 ºC [139]. This contradiction with previous studies was explained by the higher ionic conductivity of the Co-rich LSCF0.2 compared to LSCF0.8. The authors concluded that the introduction of an ionic conductive but electrocatalytically inactive CGO phase was detrimental to the electrochemical performance of nanostructured LSCF0.2.

By using an alternative strategy, a honeycomb microstructure, comprising macro- and micro-pores, was prepared by electrostatic slurry spray deposition for the $Sm_{0.5}Sr_{0.5}CoO_3$-$Ce_{0.8}Sm_{0.2}O_{2-\delta}$ composite cathode [140]. The polarization resistance was significantly decreased, ~0.1 Ω cm^2 at 750 ºC, compared to a conventional screen-printed cathode ~0.6 Ω cm^2. Further investigations were carried out by adding polyvinyl pyrrolidone as additive to a $La_{0.6}Sr_{0.4}CoO_{3-\delta}$-CGO composite slurry, which was then deposited by electrospray deposition onto a NiO-YSZ/YSZ/CGO cell, obtaining crack free cathode layers. The maximum power density was of ~0.8 W cm^{-2} at 650 °C [141].

Such results indicate that the preparation of nanocomposite by spray routes is a promising strategy to obtain efficient cathodes for SOFCs in only one preparation step, simplifying notably the fabrication process. The main advantage of nanocomposites electrodes is their microstructural stability at high operation temperatures; however, new compositions and the durability after long term operation need to be further investigated.

3.4. Graded and multilayered cathodes

It is well known that the contact quality and electrical properties between two different layer materials may be tailored by gradually changing the composition or porosity between them. Each individual layer needs to be graded in a way that enables a constant and smooth transition from one pure compound to the other one. The generated gradient minimizes the thermal expansion coefficient mismatch between the electrolyte and the electrode materials, improving the mechanical stability.

Gradient porous LSM cathodes, with ~30 μm thickness, were prepared by USP by optimizing the deposition parameters. By using a dilute organic solution, a thin layer of LSM was first deposited on YSZ, followed by three gradient porous layers sprayed from a concentrated solution at higher temperatures [93].

Recently, Sharma *et al.* prepared a graded composite based on the combination of different Ruddlesden-Popper phases with composition $La_{n+1}Ni_nO_{3n+1}$ (n=2 and 3) [142]. In order to achieve a gradient composite, first a dense and a coral-type layer of La_2NiO_4 were deposited by ESD on YSZ electrolytes, followed by screen-printing layers of La_2NiO_4:$La_3Ni_2O_{7+\delta}$ or La_2NiO_4:$La_4Ni_3O_{10-\delta}$, which partially penetrated into the coral-type layers. Finally, current collector layers of $La_3Ni_2O_{7+\delta}$ or $La_4Ni_3O_{10-\delta}$ were screen-printed, obtaining the graded composites. The polarization resistance was as low as 0.21 Ω cm^2 at 600 ºC, showing better electrochemical performance than the homogenous La_2NiO_4:$La_4Ni_3O_{10-\delta}$ (50:50 wt.%) composite cathode, 0.50 Ω cm^2 at 600 ºC. Moreover, the graded composite cathodes showed a good stability at 650 ºC for 15 days.

Further research on gradient composite cathodes were carried out by Lee *et al.* by depositing $Sm_{0.5}Sr_{0.5}CoO_{3-\delta}$-$BaCe_{0.7}Zr_{0.2}Y_{0.1}O_{3-\delta}$ (SSC-BCZY) by electrostatic spray slurry deposition, gradually decreasing the BCZY-content (Fig. 5b). The graded composites greatly improved both the ohmic and polarization resistances of an anode supported cell [143]. Later on, the same research group developed a gradient porous composite based on $La_{0.6}Sr_{0.4}Co_{0.2}Fe_{0.8}O_{3-\delta}$-$BaCe_{0.7}Zr_{0.15}Y_{0.15}O_{3-\delta}$ (LSCF-BCZY) that drastically reduced the polarization resistance, especially for the low frequency process of the impedance spectra, assigned to the charge-transfer reaction on the electrode surface. In order to obtain a graded porosity, two separated solutions of LSCF-BCZY and super P carbon black as pore former were prepared. The flow rate of the pore former solution was changed during spray deposition to tailor the porosity [144].

Holtappels and Bagger prepared two graded electrode configurations consisting of 5 and 9 layers of YSZ-LSM and LSM-LSC [145]. A precursor solution with low LSM content was firstly deposited on the electrolyte and the subsequent YSZ-LSM/LSM-LSC layers were graded in composition. The graded cathode showed a homogenous distribution of pores and particles. In such configuration, the composition smoothly changed in the whole thickness of the cathode, allowing a soft transition between the three materials. The electrochemical performance of these graded electrodes was considerably enhanced, R_p=0.2 Ω cm^2 at 750 ºC, due to the improved functionality of each individual layer. Hence, the enhanced performance of the graded cathodes was attributed to the optimized interfaces, combined with the better current collection of the LSC films close to the active layers.

In 2019, an innovative electrode architecture consisting in alternating layers of LSCF and CGO was prepared by CSD [146]. Two different precursor solutions of each material were supplied

independently by two syringe pumps, and alternatively sprayed onto the CGO substrates. The resulting multilaminated material was highly porous with vertical channels that guaranteed a good oxygen diffusion inside the electrode (Fig. 5c). The polarization resistance decreased with the number of LSCF/CGO bilayers, i.e. 0.38 and 0.11 Ω cm^2 at 600 ºC for the blank LSCF and five LSCF/CGO bilayers, respectively. These values were relatively low compared to those of a screen-printed LSCF-CGO composite cathode, 2.1 Ω cm^2. The electrocatalytic improvement was attributed to the extended TPB due to a higher contact area between LSCF and CGO materials. Moreover, the CGO layers acted as a protective coating to prevent the carbonation of the LSCF surface that usually blocks the catalytic sites for ORR after long term operation [147-149]. The authors concluded that this novel strategy may be employed to prepare different cathode and anode materials with enhanced stability and performance.

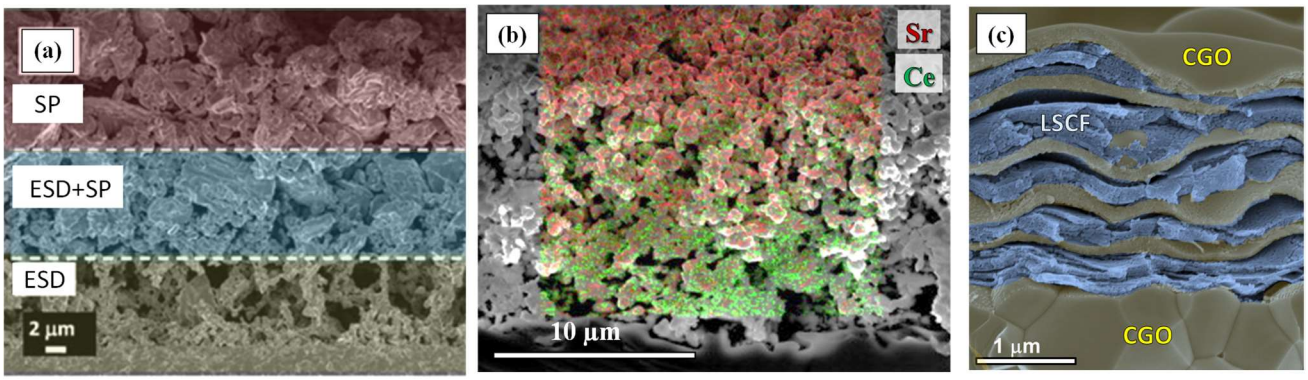

Fig. 5. (a) SEM image of the functionally graded $La_{n+1}Ni_nO_{3n+1}$ (n= 1 and 2) cathode deposited by ESD with a screen-printed (SP) La_2NiO_4 cathode [142], Copyright 2017 Royal Society of Chemistry. (b) Combined SEM and EDX mapping of a $Sm_{0.5}Sr_{0.5}CoO_{3-\delta}$-$BaCe_{0.7}Zr_{0.2}Y_{0.1}O_{3-\delta}$ gradient composite cathode prepared by ESD [143], Copyright 2014 Elsevier, and (c) SEM image of the LSCF-CGO multilayer composite cathode obtained by CSD [146], Copyright 2019 Elsevier.

3.5. Nanostructured cathodes deposited onto porous backbones

In the last few years, the infiltration method is one of the most employed procedures to develop highly efficient cathodes. In such approach, a porous electrolyte backbone is formed on a dense electrolyte, and then a precursor solution containing the stoichiometric metal salt precursors of the catalyst material is infiltrated into the porous backbone [38,150,151]. After successive infiltration/thermal treatments, a nanostructured electrode is formed on the backbone surface (Fig. 2f). By this way, electrodes with an extended TPB length are obtained, which are more efficient at low operating temperatures [152-155]. This method has been widely used in small lab-scale research; however, its implementation at large-scale is complicated for two reasons: (i) multiple impregnation and heat treatments cycles are needed to achieve a sufficient conductivity and stability of the infiltrated

electrodes, resulting in a high time consumption and cost; and (ii) it is difficult to obtain a homogeneous distribution of the catalytic material by manual dropwise addition over large areas.

In 2015, an alternative approach to the classical infiltration method was developed by dos Santos-Gómez *et al*., which consisted on depositing the cathode precursor solution by CSD onto the surface of a porous electrolyte backbone [123]. To ensure a good penetration of the precursor salts, the deposition temperature was as low as 200 ºC. A double layer electrode was obtained; the inner layer was a porous backbone homogeneously coated by the active material that provided a high TPB density for ORR, whereas, the top layer was formed exclusively by nanoparticles of a MIEC that improves the current collection (Fig. 6a-b). The thickness of both the superficial layer and the backbone coating were tailored by changing the deposition temperature and time. This strategy was employed with different cathode materials, such as $La_{0.6}Sr_{0.4}Co_{1-x}Fe_xO_{3-\delta}$ (x = 0, 0.2, 0.8 and 1) on CGO electrolytes (Table 4). Low R_p values were obtained, e.g. 0.18 Ω cm^2 for LSF, 0.078 Ω cm^2 for LSCF and 0.071 Ω cm^2 for LSC, at 600 ºC [156]. These values were lower than those obtained for related cathode materials prepared by the wet-infiltration method. In another study, the layered perovskite $PrBaCo_2O_{5+\delta}$ (PBC), deposited onto a porous CGO backbone by CSD, showed a polarization resistance of only 0.027 Ω cm^2 at 600 ºC compared to 0.22 Ω cm^2 for the same cathode prepared by screen-printing. A remarkable peak power density of 0.95 W m^{-2} at 600 ºC was obtained for the nanostructured PBC cathode in a Ni-CGO/CGO/PBC cell [107]. Even more interesting, the nanostructured PBC achieved improved durability, with stable R_p values after 600 h of operation (Fig. 6c). The authors concluded that this innovative approach involves some advantages in comparison to the classical wet infiltration method: (i) the temperature may be changed during the deposition process to decompose in-situ the precursor salts, reducing preparation steps, costs and time; (ii) a more homogeneous distribution of the catalytic material over large area is possible; and (iii) a shadow mask may be employed to cover a specific surface of the electrolyte.

A similar strategy was used by Sharma *et al.* [157]. A porous CGO backbone was first deposited on a CGO electrolyte, and then coated with a $Ln_2NiO_{4+\delta}$ (Ln=La, Pr) porous layer by EDS that partially penetrated into the CGO backbone, leading to a CGO-$Ln_2NiO_{4+\delta}$ composite. Finally, a $Ln_2NiO_{4+\delta}$ current collector layer was deposited by screen-printing. This triple layer electrode architecture showed stable polarization resistances of 0.08 and 0.03 Ω cm^2 at 650 ºC for $La_2NiO_{4+\delta}$ and $Pr_2NiO_{4+\delta}$, respectively.

Song *et al.* recently reported an epitaxial deposition of $Sm_{0.5}Sr_{0.5}CoO_{3-\delta}$ (SSC) infiltrated into $La_{0.6}Sr_{0.4}Co_{0.2}Fe_{0.8}O_{3-\delta}$-$Ce_{0.8}Gd_{0.2}O_{1.9}$ cathodes via USD (Fig. 6d) [158]. The infiltrated cathode showed a dramatic decrease of the ohmic and polarization resistance, whereas only a slight improvement was achieved for those electrodes prepared by the traditional infiltration approach. TEM

analysis revealed an epitaxial growth of SSC on the surface of the LSCF cathode, which explained the performance improvement (Fig. 6e). In addition, no appreciable degradation was observed after 300 h of operation. The SSC infiltrated LSCF-CGO cathode showed a maximum power density of 0.79 W cm^{-2} at 800 ºC compared to 0.34 W cm^{-2} for the same cell with the non-infiltrated cathode (Fig. 6f).

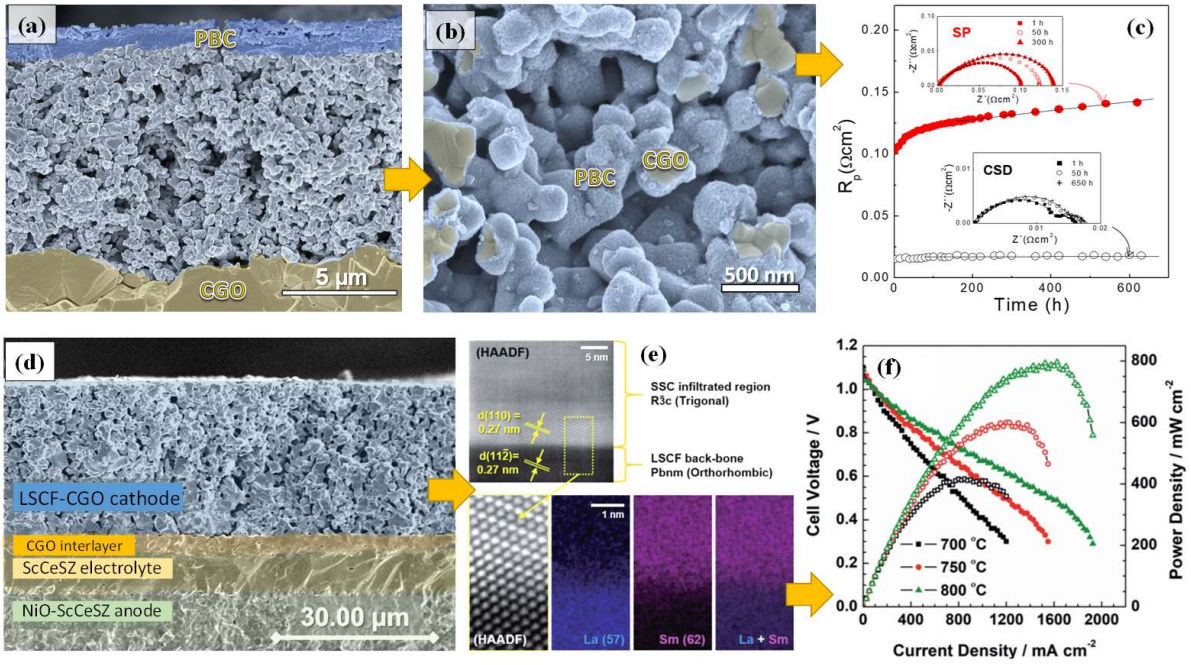

Fig. 6. (a, b) SEM images at different magnifications of a $PrBaCo_2O_{5+\delta}$ cathode infiltrated into CGO backbone by CSD, and (c) variation of the polarization resistance over time for cathodes obtained by CSD and traditional screen-printed (SP) at 650 ºC. The inset figures show the impedance spectra at different times [107], Copyright 2017 Royal Society of Chemistry. (d) Cross-sectional SEM image of a NiO-ScCeSz/ScCeSZ/CGO/LSCF-CGO anode-supported cell, (e) HAADF-STEM image showing the epitaxial growth of $Sm_{0.5}Sr_{0.5}CoO_3$ cathode deposited by USD into LSCF backbone and (f) voltage-power density curves of the single cell [158], Copyright 2020 Royal Society of Chemistry.

$BaCO_3$ nanoparticles, which have demonstrated excellent catalytic activity for ORR [159], were also infiltrated by USD into LSCF and LSCF-SDC cathodes. For this purpose, a precursor solution of barium acetate, modified by a surfactant (Triton™X-100), was used [160]. The polarization resistance of $BaCO_3$-infiltrated LSCF was of 1.2 Ω cm^2 at 700 ºC and increased only 1.6% after 500 h.

Spray-coating has been also employed to control the surface phase segregation in perovskite-based electrodes [147]. It has been reported that alkaline-earth containing cathodes, such as LSCF, are susceptible to surface phase segregations [161], which are usually related to electrostatic effects and the structural stress generated in the crystal structure when large cation dopants are incorporated into the lattice. In particular, Sr-enrichment on the surface of LSCF leads to a deactivation of oxygen dissociative adsorption and, consequently, the performance decreases over time. In this context, the durability of LSCF may be improved by superficial modifications. For instance, Lynch *et al*. observed enhanced durability and performance in a LSCF cathode coated with LSM particles [162]. Similarly,

Gong *et al*. have found that the performance of LSCF-CGO was retained by coating the electrode surface with a ZrO_2 film by atomic layer deposition [163].

Table 3. Electrode properties of cathodes prepared by using different strategies by spray-pyrolysis deposition and techniques. Polarization resistance in air and power densities are given at 600 ºC. In those cases, where not data are available at 600 ºC, the temperature is included

Strategy	Composition	Abbreviation	Preparation	Thickness (µm)	Particle size (nm)	Electrolyte	R_p^{air} (Ω cm^2)	P (W cm^{-2})	Ref.
Nanocomposite	$La_{0.8}Sr_{0.2}MnO_{3-\delta}$ + $Ce_{0.9}Gd_{0.1}O_{1.95}$	LSM-CGO	CSD	--	15	YSZ	0.29	0.29	130
Nanocomposite	$La_{0.6}Sr_{0.4}Co_{0.2}Fe_{0.8}O_{3-\delta}$ + $Ce_{0.8}Gd_{0.2}O_{1.9}$	LSCF-CGO	CSD	0.15-0.35	3-30	YSZ	2	--	131
Nanocomposite	$La_{0.6}Sr_{0.4}Co_{0.2}Fe_{0.8}O_{3-\delta}$ + $Ce_{0.8}Gd_{0.2}O_{1.9}$	LSCF-CGO	CSD	0.25-0.30	15-50	YSZ	3	--	132
Nanocomposite	$La_{0.6}Sr_{0.4}Co_{0.2}Fe_{0.8}O_{3-\delta}$ + $Ce_{0.9}Gd_{0.1}O_{2-\delta}$	LSCF-CGO	ESD	4-6	<100	CGO	0.13	--	137
Nanocomposite	$La_{0.6}Sr_{0.4}Co_{0.2}Fe_{0.8}O_{3-\delta}$ + $Ce_{0.9}Gd_{0.1}O_{1.95}$	LSCF-CGO	CSD	6	30-50	CGO	0.16	0.71	138
Nanocomposite	$La_{0.6}Sr_{0.4}Co_{0.8}Fe_{0.2}O_{3-\delta}$ + $Ce_{0.9}Gd_{0.1}O_{2-\delta}$	LSCF-CGO	ESD	2	45	CGO	2.75	--	139
Nanocomposite	$Sm_{0.5}Sr_{0.5}CoO_{3-\delta}$ + $Ce_{0.8}Sm_{0.2}O_{2-\delta}$	SSC-CSO	ESD	20	--	CSO	0.1 (750ºC)	--	140
Graded	$La_2NiO_{4+\delta}$ − $La_4Ni_3O_{10}$	--	ESD	30	150-800	CGO	0.22	--	142
Graded	$La_2NiO_{4+\delta}$ − $La_3Ni_2O_7$	--	ESD	30	150-450	CGO	0.21	--	142
Graded	$Sm_{0.5}Sr_{0.5}CoO_{3-\delta}$-$BaCe_{0.7}Zr_{0.2}Y_{0.1}O_{3-\delta}$	SSC-BCZY	ESD	20	-	BCZY	0.23	0.41 (700 ºC)	143
Multilaminated	$La_{0.6}Sr_{0.4}Co_{0.2}Fe_{0.8}O_{3-\delta}$ + $Ce_{0.9}Gd_{0.1}O_{1.95}$	LSCF-CGO	CSD	5	30	YSZ	0.11	-	146
Infiltrated	$La_{0.8}Sr_{0.2}MnO_{3-\delta}$	LSM	CSD	10	--	CGO	0.18	--	123
Infiltrated	$Ce_{0.8}Gd_{0.2}O_{1.9}$	LSCF	CSD	15	30	CGO	0.25	0.5	147
Infiltrated	$La_{0.6}Sr_{0.4}FeO_{3-\delta}$	LSF	CSD	10	--	CGO	0.18	--	156
Infiltrated	$La_{0.6}Sr_{0.4}Co_{0.8}Fe_{0.2}O_{3-\delta}$	LSCF	CSD	10	--	CGO	0.078	--	156
Infiltrated	$La_{0.6}Sr_{0.4}CoO_{3-\delta}$	LSC	CSD	10	--	CGO	0.071	--	156
Infiltrated	$PrBaCo_2O_{5+\delta}$	PBC	CSD	11	<50	CGO	0.027	0.95	107
Infiltrated	$La_{0.6}Sr_{0.4}Co_{0.2}Fe_{0.8}O_{3-\delta}$/ $Sm_{0.5}Sr_{0.5}CoO_{3-\delta}$	LSCF/SSC	UPD	30	--	$Sc_{0.10}Ce_{0.01}Zr_{0.89}O_2$	-	0.79 (800 ºC)	158
Infiltrated	$BaCO_3$ nanoparticles	$BaCO_3$	USD	--	100	CGO	1.2	--	159
Infiltrated	$BaCo_{0.4}Fe_{0.4}Zr_{0.1}Y_{0.1}O_{3-\delta}$	BCFZY	CSD	--	30-80	CGO	0.067	1.0	110
Infiltrated	$La_2CuO_{4+\delta}$	LCO	CSD	12	220	CGO	0.14	--	105

In 2017, LSCF-CGO cathodes were successfully coated with a CGO thin film by CSD [147]. The coated cathodes presented lower degradation rate over time, as well as lower R_p values due to the protective effects of CGO coating and the extended TPB. These protective coatings were only effective at temperatures lower than 800 ºC due to the grain growth and coarsening at higher annealing temperature. An anode supported cell with the protected cathode showed a power density of 0.50 W cm^{-2} at 600 ºC compared to 0.39 W cm^{-2} for the same cell with the uncoated cathode. The authors

concluded that the CGO coating approach may be used with a wide range of electrodes containing alkaline-earth elements to improve the durability and performance of the cell. This coating strategy might also be used to prevent chromium poisoning from the interconnector materials, as well as to improve the stability of the anode materials against carbon deposition and sulphur poisoning.

Table 3 compares the properties of several cathodes prepared using the different microstructural strategies discussed in sections 3.2-3.5. In general, the best results, with the lowest values of polarization resistance, were obtained for the infiltrated electrodes. For instance, LSM deposited directly on a YSZ electrolyte, LSM-CGO nanocomposite and LSM infiltrated into a YSZ backbone exhibited R_p values of 1.8, 0.29 and 0.18 Ω cm^2 at 600 ºC, respectively.

3.6. Cathodes with functional and active layers.

Active functional layers, i.e. a composite material or a nanostructured layer with good electrochemical activity for ORR, are usually introduced between the electrolyte and the cathode to improve the performance [164]. Moreover, the use of thin active interlayers is also a useful strategy to improve the charge transfer reactions at the electrode/electrolyte interface. Since different electrochemical processes take place at the interfaces between the different SOFC components, they play an important role on the electrode performance. In this section, functional and active layers prepared by spray-pyrolysis techniques are discussed.

In 2016, Sharma *et al.* reported a novel microstructural design consisting on $Ln_2NiO_{4+\delta}$ (LnNO; Ln = La, Pr) thin films prepared by ESD, followed by a screen-printed cathode with the same composition [157,165]. The R_p values decreased from 3.33 to 0.08 Ω cm^2 at 600 °C for PrNO cathode without and with the functional layer, respectively. The active functional layer not only enhanced the electrochemical properties but also provided stable R_p values over time. Similarly, Khamidy *et al.* prepared active layers of $LaPrNiO_{4+\delta}$ (LPNO) by combining ESD and screen-printing deposition, obtaining electrodes with a low polarization resistance, ~0.20 Ω cm^2 at 600 ºC [166,167]. Recently, $La_{2-x}Pr_xNiO_{4+\delta}$ (x = 0, 0.5, 1 and 2) layers have been also prepared by ESD, consisting of a dense layer (~100 nm) and a 3D coral microstructure (~20 μm), topped by a screen-printed current collector of the same composition [168]. The results revealed that $LaPrNiO_{4+\delta}$ showed the best compromise between electrochemical properties and stability, achieving rather low R_p values, 0.12 Ω cm^2 at 600 ºC, and a maximum power density of 0.44 W cm^{-2} at 700 ºC in an Ni-YSZ/YSZ/CGO anode supported cell [168].

An interesting functional layer based on Pr_6O_{11} was proposed in 2018 by Sharma *et al.* Layers with different morphologies, i.e. thick, thin, reticulated, coral and columnar type, were prepared by

ESD [169]. Single Pr_6O_{11} phases with fluorite-type structure were obtained after calcination at 700 ºC for 2 h without any evidence of reactivity with the CGO electrolyte up to 800 ºC. A double electrode layer, composed by a Pr_6O_{11} porous columnar microstructure by ESD topped by a LSCF screen-printed current collector layer, achieved one of the lowest R_p value reported so far, 0.02 Ω cm^2 at 600 ºC. A Ni-YSZ/CGO single cell with such double layer architecture showed a maximum power density of 0.5 W cm^{-2} at 700 ºC (Fig 7a-b). Since the electronic conductivity of Pr_6O_{11} is rather low (1.3 S cm^{-1} at 600 ºC [170]), the same research group investigated the influence of the current collector layer (Pr_6O_{11}, LSM and LSCF) and the morphology of Pr_6O_{11} on the electrochemical performance [171]. The polarization resistance increased with the sintering temperature, suggesting that the surface area of Pr_6O_{11} is the key parameter for its high performance. The composition and thickness of the current collector layer had a strong influence on the electrode polarization. The best result was found for a 30 μm thick LSM screen-printed layer with a polarization resistance of 0.02 Ω cm^2 at 600 ºC, similar to that reported previously for a LSCF current collector layer [169].

LSCF, with high mixed ionic-electronic conductivity, has also been investigated as active layer for SOFCs. In particular, Castro-Robles *et al.* studied the conductivity of $La_{1-x}Sr_xCo_{0.2}Fe_{0.8}O_{3-\delta}$ ($0 \leq x \leq 0.4$) deposited by ESD onto rough glass [172]. Single orthorhombic phases were obtained for all compositions up to x=0.4. The conductivity increased with the Sr-content ($0 \leq x \leq 0.4$) from 4.2 to 67.1 S cm^{-1} at 250 ºC. These results suggested that a nanostructured LSCF could be implemented as active layers for SOFCs. Çelikbilek *et al.* prepared a double-layer cathode, consisting in a 10 μm thick LSCF functional layer deposited by ESD and a LSCF current collector [173]. The microstructure of the active layer provided columnar channels for effective oxygen diffusion (Fig. 7c-d). The R_p value of this electrode was 0.037 Ω cm^2 at 650 ºC and an anode supported cell with such configuration exhibited a peak power density of 1.4 W cm^{-2} at the same temperature (Fig. 7e). These improvements were attributed to the large surface area of the active layer for ORR.

In 2019, Shin *et al.* prepared $La_{0.6}Sr_{0.4}CoO_{3-\delta}$ (LSC) and LSC-CeO_2 nanocomposite interlayers by ESD to improve the oxide-ion transport and the mechanical adhesion to the LSC cathode [174]. The LSC–CeO_2 layer exhibited high TPB length due to grain growth suppression in nanocomposite materials, leading to a particle size below 20 nm, which was much smaller than the 80 nm for LSC layers. Ni-YSZ/YSZ/CGO anode supported cells were fabricated with a protective CGO buffer layer to prevent reactivity between the LSC cathode and the YSZ electrolyte (Fig. 7f). The cells with LSC-CeO_2 and LSC interlayers showed improved SOFC performances, reaching peak power densities of 1.15 and 1.08 W cm^{-2} at 650 °C, respectively, which was 18% higher than a reference cell without an interlayer (Fig. 7g). Similarly, a bifunctional layer of CGO and $LaNi_{0.6}Fe_{0.4}O_3$, deposited by CSP, was tested in YSZ-based SOFCs [175]. The introduction of the bifunctional layer led to an improved contact between the electrolyte and the porous cathode, resulting in a decrease of both the ohmic and

polarization resistances of the cell. A Ni-YSZ/YSZ/CGO/LNF cell generated a power density of 1 W cm^{-2} at 800 ºC.

Zamudio *et al*. have prepared active interlayers of the fast-ionic conductor $Bi_{1.5}Y_{0.5}O_{3-\delta}$ (BYO) by CSD [176]. The incorporation of a BYO interlayer between YSZ electrolyte and LSM cathode decreased the resistances of both high- and low-frequency contributions of the impedance spectra, suggesting that the active layer not only improved the charge transfer at the electrolyte interface but also extended the surface path of the electrochemical reaction sites. A nanostructured LSM cathode deposited directly by CSP on YSZ electrolyte exhibited a polarization resistance of 1.15 Ω cm^2 at 600 ºC compared to 0.55 Ω cm^2 for the same cathode with a BYO active layer.

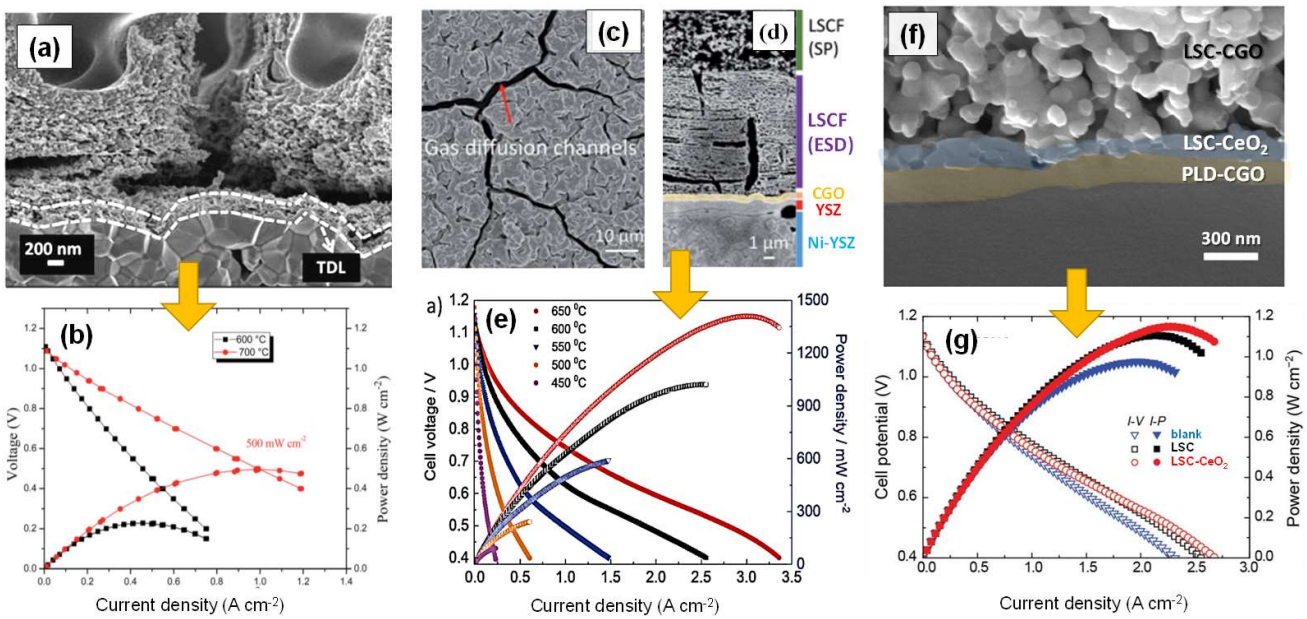

Fig. 7. (a) SEM images of Pr_6O_{11} active functional layer obtained by ESD and (b) voltage-power density curves at 600 and 700 ºC for a NiO-CGO/CGO/Pr_6O_{11}/LSCF cell [169], Copyright 2018 Royal Society of Chemistry. (c) Surface image of a LSCF active functional layer obtained by ESD, (d) cross-sectional SEM image of a Ni-YSZ/YSZ/CGO/LSCF cell and the corresponding (e) voltage-power density curves at different temperatures [173], Copyright 2019 Royal Society of Chemistry. (f) SEM image of a double active layer formed by a CGO and LSC-CeO_2 films obtained by pulsed-laser deposition and CSD, respectively. (g) Voltage-power density curves of the Ni-YSZ/YSZ/CGO/LSC-CGO cells with LSC and LSC-CeO_2 active layer and blank cell without active layer [174], Copyright 2019 Elsevier.

Recently, Zapata-Ramírez *et al*. employed the CSD technique to obtain dense active layers of $Ce_{0.8}Gd_{0.2}O_{2-\delta}$ (CGO), $Ce_{0.8}Pr_{0.2}O_{2-\delta}$ (CPO) and $SrFe_{0.9}Mo_{0.1}O_{3-\delta}$ (SFM) of approximately 300 nm thickness between the CGO electrolyte and the screen-printed SFM cathode [177]. Considerable modifications in the serial and polarization resistances were observed, especially in the low temperature range due to the different transport properties of the interlayers. The best results were

achieved for a CPO active interlayer due to its higher mixed ionic-electronic conductivity, increasing the surface path for the electrochemical reactions. Similarly, the electrical properties of the LSCF cathode were investigated in contact with active layers of $Sm_{0.5}Sr_{0.5}CoO_{3-\delta}$ (SSC), $La_{0.6}Sr_{0.4}CoO_{3-\delta}$ (LSC), $La_{0.6}Sr_{0.4}Co_{0.2}Fe_{0.8}O_{3-\delta}$ (LSCF), and Pr_6O_{11} prepared by CSP [178]. The introduction of these interlayers also improved the contact between the electrode and the electrolyte, and consequently the electrode performance. R_p values of 0.5, 0.245, 0.137, 0.119 and 0.107 $\Omega \cdot cm^2$ at 600 ºC were obtained for cells without and with Pr_6O_{11}, LSCF, LSC and SSC interlayers, respectively, at 600 ºC. Furthermore, an anode-supported cell without and with a LSC interlayer reached maximum power densities at 600 ºC of 0.74 and 1.22 $W \cdot cm^{-2}$, respectively.

The properties of different functional and active layers prepared by spray-pyrolysis are given in Table 4.

Table 4. Properties of active and functional layers, prepared by spray-pyrolysis techniques, used with different cathodes. Polarization resistance in air and power densities are given at 600 ºC. In those cases, where not data are available at 600 ºC, the temperature is included.

Functional layer	Electrode	Deposition	thickness (µm)	Particle size (nm)	Electrolyte	R_p^{air} (Ω cm^2)	P ($W\ cm^{-2}$)	Ref.
LNO	LNO+LNO(SP)	ESD -SP	40	150	CGO	0.42	--	165
LNO	LNO(SP)	ESD	--	--	CGO	0.42	--	157
LNO	LNO(SP)+CGO(SP)	ESD	--	--	CGO	0.16	--	157
Pr_6O_{11}	LSM	ESD	6	35	CGO	0.02	--	171
PNO	PNO(SP)	ESD	--	--	CGO	0.08	--	157
PNO	PNO(SP)+CGO(SP)	ESD	8	--	CGO	0.04	--	157
LPNO	LPNO	ESD	20	150	CGO	0.69	--	166
CGO	LPNO	ESD	31	150	CGO	0.20	--	166
LSCF	LSCF	ESD	10	--	CGO	0.1	1.00	173
LSC	LSC	ESD	--	--	YSZ/CGO	0.169 (650ºC)	1.11(650ºC)	174
LSC + CeO_2	LSC-CeO_2	ESD	--	20	YSZ/CGO	0.171 (650ºC)	1.15 (650ºC)	174
BYO	LSM(SP)	CSD	0.2	--	YSZ	0.55 (650ºC)	--	176
SFM	SFM+CGO(SP)	CSD	0.2-0.4	20	CGO	1.90	--	177
CGO	SFM+CGO(SP)	CSD	0.2-0.4	20	CGO	0.80	--	177
$Ce_{0.8}Pr_{0.2}O_{2-\delta}$(CPO)	SFM+CGO(SP)	CSD	0.2-0.4	20	CGO	0.30	--	177
LSCF	LSCF	CSD	0.4	$28^{700\,ºC}$	CGO	0.137	-	178
Pr_6O_{11}	LSCF	CSD	0.5	$49^{700\,ºC}$	CGO	0.245	-	178
$La_{0.6}Sr_{0.4}CoO_{3-\delta}$	LSCF	CSD	0.5	$23^{700\,ºC}$	CGO	0.119	1.21	178
$Sm_{0.5}Sr_{0.5}CoO_{3-\delta}$	LSCF	CSD	0.6	$27^{700\,ºC}$	CGO	0.107	-	178
CGO	LSCF	CSD	0.15	33.6-84.5	YSZ	0.42 (700ºC)	--	183
CGO	LSCF	CSD	0.3	--	YSZ	0.154 (750ºC)	0.73 (750ºC)	184
CGO	LSCF	CSD	0.7	--	YSZ	0.114 (750ºC)	0.99 (750ºC)	184
CGO	LSCF	CSD	1.5	--	YSZ	0.106 (750ºC)	0.81 (750ºC)	184
$Ce_{0.6}La_{0.4}O_{2-\delta}$(LDC)	Ni-YSZ	FSD	5	--	LSGM	--	0.04	186
LDC	NiO-CGO	FSD	--	--	LSGM	1.0	0.46 (750ºC)	187

3.7. Doped-ceria protective and active interlayers

As aforementioned, the elevated operating temperature of SOFCs may cause stability issues after long-term operation due to cation interdiffusion and chemical reactivity between the material layers of the cell [179]. A possible solution to mitigate the thermal incompatibility between the cell components is the introduction of a protective buffer layer. Such nanostructured protective layers not only avoid the reactivity between the materials but also improve the electrode performance due to better adhesion and charge transfer reactions between the electrolyte and electrodes.

The most commonly used buffer layers are those based on doped-CeO_2 due to its better compatibility with efficient cathodes, such as LSCF, BSCF and PBC, which are chemically incompatible with YSZ electrolyte [180]. These interlayers need to be sufficiently thin and dense to avoid the introduction of additional ohmic losses. Traditionally, CGO layers are prepared by screen-printing; however, sintering temperatures as high as 1200-1400 ºC are required, leading to cation interdiffusion between materials [180]. Thus, dense CGO buffer layers need to be prepared at reduced temperatures. Among the different physical and chemical deposition methods to obtain CGO protective layers, spray pyrolysis has been widely investigated due to the previously mentioned advantages, i.e. no-vacuum process, economic and scalable technique, among others.

The microstructural evolution with the annealing temperature of CGO layers, deposited by CSD, was widely studied by Gauckler *et col.* [181,182]. The as-deposited layers were amorphous at 370 ºC. SEM images of CGO films revealed a ~50 vol.% porosity up to 800 ºC, attributed to the decomposition of the organic compounds employed in the precursor solution. Fully dense CGO films were obtained at temperatures higher than 1000 ºC. Later, dos Santos-Gómez *et al*. prepared CGO films by CSD, employing aqueous precursor solutions of acetate, chloride and nitrate salts at a deposition temperature of 450 ºC [183]. This temperature is significantly lower than that used by traditional screen-printed method, 1200 ºC, avoiding cation interdiffusion between the YSZ and CGO layers. In particular, acetate salts provided dense CGO layers with enhanced morphological features after deposition and annealing at 450 ºC, i.e. 1.5 nm of roughness, uniform thickness of about 300 nm and good adherence. Such films were evaluated as protective layers in LSCF/YSZ/LSCF symmetrical cells. The cell with protective CGO layers exhibited a stable R_p value of 0.42 Ω cm^2 at 750 ºC. In contrast, the same cells without CGO interlayers suffered a drastic increase of R_p from 1 to 36 Ω cm^2 after 150 h of operation.

Further insights about CGO barrier layers deposited by CSD onto YSZ substrates were carried out by Molin *et al.* in 2020 [184]. Thin and dense CGO layers with different thicknesses (300, 700 and 1500 nm) were prepared. The power output generated for a NiO-YSZ/YSZ/CGO/LSCF cell was dependent on the CGO layer thickness. The best performance was found for the 700 nm thick CGO film, showing the lowest ohmic and polarization resistances as well as better stability over time. The

authors found that thin films (300 nm) are not effective to prevent cation interdiffusion, due to delaminations of the CGO layers, whereas thicker barrier layers (1500 nm) negatively affect the total ohmic resistance of the cells.

Other authors have also obtained dense CGO protective layers prepared by CSD to prevent the reaction between the electrolyte and electrodes. For instance, Stoermer *et al*. prepared CGO buffer layers deposited between the LSM cathode and the YSZ electrolyte by CSD, which avoided the formation of an insulating $La_2Zr_2O_7$ and the degradation of the cell [185].

Ma *et al*. have introduced a La-doped CeO_2 (LDC) thin film as interlayer by plasma spray between a NiO-YSZ anode and a LSGM electrolyte, preventing the formation of $LaNiO_3$ [186]. Wang *et al*. have also confirmed that LDC films prepared by plasma spray were effective interlayers to avoid reactions between Ni-based anodes and LSGM electrolytes. The cell with such buffer layer showed a constant performance at 650 ºC, confirming the suppression of the interfacial reactivity [187].

Several authors have prepared CGO protective layers by other spray-based techniques. Karageorgakis *et al*. deposited dense and homogenous CGO thin films by FSD deposition [188]. Rossignol *et al*. obtained continuous, crack-free and dense CGO films by ESD with a thickness of only 85 nm [189]. Constantin *et al*. have applied the ESD technique to prepare CGO thin films on YSZ substrates, without visible reaction between YSZ and LSCF at an annealing temperature of 800 ºC [190]. All these results verify that spray techniques are an effective method to obtain dense and nanostructured CeO_2-based interlayers to prevent reactivity between cell components, as well as improving the electrode performance.

4. Anode and symmetrical electrodes

Regarding the preparation of anode materials by spray pyrolysis techniques, most of the investigations are devoted to the preparation of Ni-YSZ and Ni-CGO powders [191-200] with spherical or core-shell morphologies. In general, these anodes exhibit improved electrochemical performance in terms of lower overpotential and ohmic losses, when compared to traditional Ni-cermets obtained by mixing powders. In addition, the better homogeneity of these anodes helps to suppress the Ni coarsening. For instance, Kawano *et al*. reported an easy way to control the morphology and composition of NiO-$Ce_{0.9}Sm_{0.1}O_{1.95}$ (NiO-CSO) anodes by CSD. Either citric acid or nitric acid were added to the nitrate starting solution, obtaining a highly dispersed NiO and CSO spherical or instead capsule-type particles, where NiO was covered with a thin CSO layer. The performance of the cell fabricated with highly dispersed particles was slightly better than the cell fabricated with capsule-type particles [195]. A single cell based on Ni-GDC presented an almost negligible degradation after 500 h of operation [192]

Related to thin film anodes, Liu *et al.* deposited Ni-CGO films onto YSZ substrates by ESD. In order to control the microstructure and porosity of the anode, the deposition temperature, time, precursor solution concentration and feed rate were varied [201]. It was found that the particle size increased from 2 to 20 μm when the concentration of the precursor solution was also increased from 0.025 to 0.4 mol L^{-1} at 250 ºC (Fig. 8a-d). Furthermore, the particle size and the porosity increased and decreased with an increasing deposition temperature due to a fast evaporation rate of the solvent [202]. The authors also commented that temperatures above 450 ºC should be avoided due to crack and delamination of the layers as consequence of the high thermal stress. Further investigations on the electrochemical properties of Ni-CGO onto YSZ were carried out by the same authors in the above-mentioned conditions. A Ni–CGO/YSZ/Ni–CGO symmetrical cell showed a considerable decrease of the polarization resistance (5.25 to 0.61 Ω cm^2 at 763 ºC) and the activation energy (from 1.06 to 0.86 eV) when the particle size was decreased from 17 to 1.5 μm [203]. Later, an electrode polarization model for the same configuration was investigated by incorporating different electrode microstructural characteristics. This model was capable of predicting the electrochemical performance, based on different microstructural variations, with a discrepancy lower than 10% [204]. Further studies were carried out by Taniguchi *et al.*, depositing NiO-CSO thin films onto CSO substrates by ESD, obtaining high porosity films at deposition temperatures between 300-350 ºC by using a precursor solution of 0.005 M with a mixture of ethanol and butyl-carbitol as solvents (1:1) [205]. Similar results were obtained for NiO-YSZ deposited by ESD using methanol as solvent [206].

The influence of the substrate on the microstructure of NiO-CGO was also studied. Different substrates were used, i.e. silicon, stainless still and glass, among which silicon wafers obtained the best results due to the lower contact angle of the aerosol drops, i.e. 25.2º, 17.3º and 5.3º, respectively [207]. In this case, the effect of the precursor solution flow rate on the film morphology was also studied. A highly porous cauliflower morphology was obtained due to the particle agglomeration at 450 ºC and flow rates of 0.7 ml h^{-1}. An increase in the flow rate to 2.8 ml h^{-1} resulted in larger aerosol droplets, diminishing the particle agglomeration, being the cauliflower morphology no longer obtained and achieving instead a continuous film. Further increasing of the flow rate up to 8.0 ml h^{-1} produced very dense and cracked films that were not suitable for SOFC anodes.

Composite anode materials with composition $La_{0.2}Sr_{0.8}TiO_3$-$Ce_{0.8}Sm_{0.2}O_{1.9}$ (LST-CSO) were prepared by both plasma spray [208] and USD [209] for LSGM electrolyte supported cells. Stability tests at 1050 ºC for 10 h in H_2, CO_2 and CH_4 humidified atmospheres showed that LST-CSO exhibited good chemical compatibility with LSGM. A 320 μm thick LSGM-supported cell showed a maximum power density of 0.3 W cm^{-2} at 800 ºC, confirming that LST-CSO deposited by USD could be a promising anode for LSGM-based SOFCs [209].

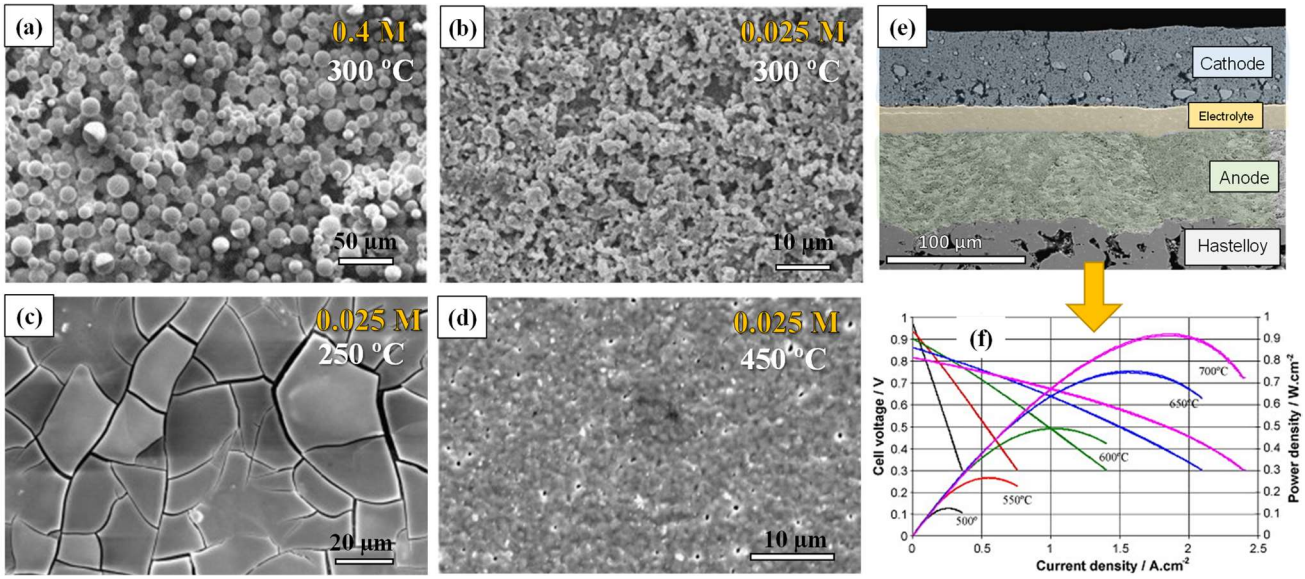

Fig. 8. (a-d) SEM images of NiO-CGO anodes deposited onto YSZ by CSD at different temperatures and precursor solution concentrations [201], Copyright 2010 Elsevier. (e) SEM image of a metal supported SOFC prepared by FSD and (f) voltage-power density curves at different temperatures [211], Copyright 2009 Elsevier.

Because of the high versatility, effectiveness and low price of spray-based techniques, this approach has been deeply studied in the fabrication of metal-supported SOFCs (Fig. 8e). Spray pyrolysis possesses the advantage that both anode and electrolyte can be deposited consecutively without a subsequent thermal treatment of the metal supported cell [210-212]. In contrast, traditional deposition methods, such as screen-printing, electrophoretic deposition or tape casting, are followed by several sintering steps, which can produce the oxidation of the metallic substrate [213]. Remarkable results were achieved for a metal-supported SOFC with a NiO-CSO/CSO/$Sm_{0.5}Sr_{0.5}CoO_3$ configuration, which rendered a maximum power density of 0.92 W cm^{-2} at 700 ºC and high stability over time (Fig. 8f) [211].

The properties of the anode materials are summarized in Table 5. The polarization resistance values for spray-pyrolysis anodes are relatively high, when compared to those reported for cathode materials. This fact is possibly due to non-optimized preparation conditions. Thus, further investigation in nanostructured anodes for SOFC is required by using the recent microstructural strategies developed for cathode materials.

Single perovskites based on Ti-doped $SrFeO_{3-\delta}$ were investigated simultaneously as both anode and cathode for symmetrical SOFCs. Layers with composition $Sr_{0.98}Fe_{1-x}Ti_xO_{3-\delta}$ (x=0, 0.2, 0.4 and 0.8) were deposited by CSD on YSZ [214]. The electrodes were stable under reducing and oxidizing atmospheres. $Sr_{0.98}Fe_{0.8}Ti_{0.2}O_{3-\delta}$ exhibited R_p values of 0.1 and 0.07 Ω cm^2 in air and H_2, respectively, at 700 ºC. A 300 µm thick LSGM electrolyte-supported cell generated a power density of 0.7 W cm^{-2}

at 800 ºC. This work confirmed that different MIECs can be prepared by spray-pyrolysis and potentially used as SOFC anodes.

Table 5. Properties of the anode materials prepared by spray-pyrolysis techniques.

Composition	Morphology	Preparation	Thickness (µm)	Particle size (nm)	Electrolyte	R_p^{air} (Ω cm^2)	P (W cm^{-2})	Ref.
NiO + CSO	Matrix and capsule type	CSP	--	--	LSGM	--	0.30 (750ºC)	195
Ni + CGO	Porous	USD	18-37	1.5-17 µm	YSZ	5.45-0.61 (663-673ºC)	--	201
$La_{0.2}Sr_{0.8}TiO_3$ + CSO	Porous	FSD	40-50	60-500	LSGM	0.53 (800ºC)	0.30 (800ºC)	208
$La_{0.2}Sr_{0.8}TiO_3$ + CSO	Porous	USD	--	0.4-3.4 µm	LSGM	--	0.14 (800ºC)	209
NiO + CSO	Porous	FSD	40	--	CSO	--	0.92 (700ºC)	211
$Sr_{0.98}Fe_{0.8}Ti_{0.2}O_{3-\delta}$	Porous CGO scaffold coated by $SFT_{0.2}$	CSD	20	50	LSGM	0.07 (700ºC)	0.7 (800ºC)	214

5. Conclusions and perspectives

The lowering of the operating temperature of SOFC devices to the range of 500-700 ºC is crucial for the widespread commercialization of this technology. However, at low temperatures, the electrochemical reactions in the electrode are not favored, despite the fact that the physical and chemical compatibility between cell components are improved. Although novel and efficient electrode materials have been developed in the last few years, e.g. $La_{0.6}Sr_{0.4}Co_{0.8}Fe_{0.2}O_{3-\delta}$, $Ba_{0.5}Sr_{0.5}Co_{0.8}Fe_{0.2}O_{3-\delta}$, $PrBaCo_2O_{5+\delta}$ and $Sm_{0.5}Sr_{0.5}CoO_{3-\delta}$, most of them suffer from certain deficiencies related to phase stability after long-term operation and chemical compatibility with the electrolyte, which may be derived from the intrinsic material properties or as a result of inadequate synthetic methods. In this context, the traditional electrode preparation, based on screen-printing, has the disadvantage of a high sintering temperature (1000-1200 ºC) needed to ensure a good adherence to the electrolyte. Such sintering temperatures result in a loss of the electrode performance and possible reactivity with the electrolyte.

The growing of electrodes directly on the electrolyte could overcome some of the critical issues related to adherence and the physical and chemical compatibility between the cell components. In this context, spray-pyrolysis is a cost effective and easily scalable technique to prepare layer materials with a wide variety of morphologies, i.e. dense, porous, cracked coral-like, flower-like, etc., by simply varying the deposition conditions, such as temperature and precursor type. This technique has been widely used in the last few years to prepare different cathode materials for SOFCs: LSM, LSCF, $La_2(Ni,Cu)O_4$, $PrBa(Co,Fe)O_{5+\delta}$, $Sr_{0.5}Sm_{0.5}O_{3-\delta}$, etc. Different microstructural strategies have been also employed to obtain nanostructure electrodes with better durability and performance, including

single phase electrodes, nanocomposite electrodes, graded electrodes, infiltrated electrodes, protective and active functional layers.

One of the main limitations of the nanostructured electrodes is their microstructural stability at elevated temperatures due to grain growth and coarsening. These drawbacks can be overcome by using nanocomposite electrodes, consisting in an intimate mixture of a mixed ionic conductor and an oxide-ion conductor. It has been found that the cosintering process limits the cation diffusion and the grain growth rate, retaining the size of the particles in the nanometric range up to 1000 ºC. This promising approach has been only employed for LSM-YSZ, LSM-CGO and LSCF-CGO systems. However, related nanocomposites might be prepared by combining materials with different crystal structures. By considering that a CGO fluorite is chemically compatible with numerous MIECs with perovskite-type structure, e.g. $SrFe_{1-x}B_xO_{3-\delta}$ (B=Mo, Ti, Nb, etc. $x<0.5$) and $La_{1-x}Sr_x(Cr,Fe,Ti)O_{3-\delta}$, they might be combined to obtain new nanocomposite electrodes (anodes and cathodes) with improved thermal stability and performance.

The performance of screen-printed electrodes could also be enhanced by introducing functional, active or buffer layers prepared by spray-pyrolysis deposition. Dense and nanostructured CGO layers avoid the reaction between different electrode materials (LSM, LSCF) and the YSZ electrolyte and also improve the charge transfer reactions at the interface between both materials. Among the different functional layers, outstanding results were obtained for Pr_6O_{11} although the stability after long-term operation in a LT-SOFC needs to be further investigated. Thus, the performance of cathodes in the low temperature range may be improved by optimizing the mixed transport properties of active interlayers.

Another promising strategy is the preparation of infiltrated electrodes by spray-pyrolysis deposition into a porous electrolyte backbone layer. This innovative concept presents several advantages compared to the conventional wet infiltration method widely used in lab scale research, which includes easier industrial implementation, preparation in one single deposition/calcination step and better reproducibility. In fact, the double layer electrode architecture, consisting of an infiltrated layer with high TPB density for ORR topped with a current collector layer, exhibited a superior performance. Moreover, this innovative approach may be applicable to other electrochemical devices, such as solid electrolyzers, batteries and supercapacitors.

It is also worth noting that the different spray-pyrolysis electrodes have been investigated with oxide-ion electrolytes (YSZ, CGO and LSGM); however, proton-conducting electrolytes (doped-$BaCeO_3$ and $BaZrO_3$) are more favorable for operating at reduced temperatures due to the higher proton conductivity in the range of 400 – 600 ºC. Thus, nanostructured electrodes are expected to be physically

and chemically more stable with proton conducting electrolytes operating at the low temperature range. In particular, the development of novel oxygen electrodes and architectures with improved adherence and performance are required in solid oxide electrolyzers (SOE) in order to avoid delamination of layers during steam electrolysis, which is one of the major degradation issues in these electrochemical devices. This opens a wide field of investigation for proton-conducting solid oxide cells.

Regarding the anode materials, most of the studies have been focused on the traditional Ni-based cermets. This fact could be explained because of the development of new cathode materials have attracted more attention from researchers in the last years, since this is generally recognized as the critical issue for the performance of LT-SOFCs. Spray-pyrolyzed Ni-cermets, formed by a homogenous distribution of the components, yield a higher TPB density, lower polarization resistance and improved redox stability. However, further investigations in nanostructured anode materials for direct hydrocarbon oxidation need to be carried out by preparing relevant electrodes, e.g. doped-$(La,Sr)TiO_3$ and $Sr(Fe,Ti)O_3$, with different architectures. Nanostructured anodes infiltrated onto a ceria backbone or nanocomposites could achieve promising results that are motivated by the previous studies on cathode materials. In any case, the nanostructured electrodes with high activity and thermal stability should remain an important and interesting research field that is essential for the commercial development of LT-SOFCs in the coming years.

Acknowledgments

This work was supported by Ministerio de Ciencia, Innovación y Universidades through the RTI2018-093735-B-I00 and UMA18-FEDERJA-033 research projects (Spain). L. dos Santos-Gómez and J. Zamudio-García thanks the Ministerio de Ciencia, Innovación y Universidades for the Juan de la Cierva Formación (FJC2018-036746-I) and FPU (FPU17/02621) grants, respectively.

References

[1] M.G. Turgut, Review of electrical energy storage technologies, materials and systems: challenges and prospects for large-scale grid storage, Energy Environ. Sci. 11 (2018) 2696-2767. https://doi.org/10.1039/C8EE01419A

[2] U.M. Damo, M. L. Ferrari, A. Turan, A.F. Massardo, Solid oxide fuel cell hybrid system: A detailed review of an environmentally clean and efficient source of energy, Energy 168 (2019) 235-246. https://doi.org/10.1016/j.energy.2018.11.091

[3] Y. Huang, M. Zhu, Y. Huang, Z. Pei, H. Li, Z. Wang, Q. Xue, C. Zhi, Multifunctional Energy Storage and Conversion Devices. Adv. Mater. 28 (2016) 8344–8364. https://doi.org/10.1002/adma.201601928

[4] Y. Zheng, J. Wang, B. Yu, W. Zhang, J. Chen, J. Qiao, J. Zhang, A review of high temperature co-electrolysis of H_2O and CO_2 to produce sustainable fuels using solid oxide electrolysis cells (SOECs): advanced materials and technology. Chem. Soc. Rev. 46 (2017) 1427-1463. https://doi.org/10.1039/C6CS00403B

[5] D. Yang, J. Ma, L. Xu, M. Wu, H. Wang, The effect of nitrogen oxides in air on the performance of proton exchange membrane fuel cell. Electrochim. Acta 51 (2006) 4039-44. https://doi.org/10.1016/j.electacta.2005.11.018

[6] B.D. Gould, O.A. Batulina, K.E. Swider-Lyons, Deactivation of Pt/VC proton exchange membrane fuel cell cathodes by SO_2, H_2S and CO_2. J. Power Sources 188 (2009) 89-95. https://doi.org/10.1016/j.jpowsour.2008.11.072

[7] Y. Zhang, R. Knibbe, J. Sunarso, Y. Zhong, W. Zhou, Z. Shao, Z. Zhu, Recent progress on advanced materials for solid-oxide fuel cells operating below 500 °C, Adv. Mater. 29 (2017) 1700132. https://doi.org/10.1002/adma.201700132

[8] Z. Gao, L.V. Mogni, E.C. Miller, J.G. Railsback, S.A. Barnett, A perspective on low-temperature solid oxide fuel cells, Energy Environ. Sci. 9 (2016) 1602-1644. https://doi.org/10.1039/C5EE03858H

[9] H. Su, Y.H. Hu, Progress in low-temperature solid oxide fuel cells with hydrocarbon fuels. Chem. Eng. J. 402 (2020) 126235. https://doi.org/10.1016/j.cej.2020.126235

[10] C. Zhao, Y. Li, W. Zhang, Y. Zheng, X. Lou, B. Yu, J. Chen, Y. Chen, M. Liu, J. Wang, Heterointerface engineering for enhancing the electrochemical performance of solid oxide cells. Energy Environ. Sci. 13 (2020) 53-85. https://doi.org/10.1039/C9EE02230A

[11] C. Sun, R. Hui, J. Roller, Cathode materials for solid oxide fuel cells: A review. J. Solid State Electrochem. 14 (2010) 1125-1144. https://doi.org/10.1007/s10008-009-0932-0

[12] S. Afroze, A.H. Karim, Q. Cheok, S. Eriksson, A.K. Azad, Latest development of double perovskite electrode materials for solid oxide fuel cells: a review. Front. Energy 13 (2019) 770-797. https://doi.org/10.1007/s11708-019-0651-x

[13] Z. Shao, S.M. Haile, A high-performance cathode for the next generation of solid-oxide fuel cells. Nature 431 (2004) 170-173. https://doi.org/10.1038/nature02863

[14] N. Mahato, A. Banerjee, A. Gupta, S. Omar, K. Balani, Progress in material selection for solid oxide fuel cell technology: A review. Prog. Mater. Sci. 72 (2015) 141-337. https://doi.org/10.1016/j.pmatsci.2015.01.001

[15] A. Tarancón, M. Burriel, J. Santiso, S.J. Skinner, J.A. Kilner. Advances in layered oxide cathodes for intermediate temperature solid oxide fuel cells. J. Mat. Chem. 20 (2010) 3799-3813. https://doi.org/10.1039/B922430K

[16] S.P. Jiang. Development of lanthanum strontium manganite perovskite cathode materials of solid oxide fuel cells: A review. J. Mater. Sci. 43 (2008) 6799-6833. https://doi.org/10.1007/s10853-008-2966-6

[17] R. Pelosato, G. Cordaro, D. Stucchi, C. Cristiani, G. Dotelli, Cobalt based layered perovskites as cathode material for intermediate temperature Solid Oxide Fuel Cells: A brief review. J. Power Sources 298 (2015) 46-67. https://doi.org/10.1016/j.jpowsour.2015.08.034

[18] N. Jaiswal, K. Tanwar, R. Suman, D. Kumar, S. Upadhyay, O. Parkash, A brief review on ceria based solid electrolytes for solid oxide fuel cells. J. Alloys Compd. 781 (2019) 984-1005. https://doi.org/10.1016/j.jallcom.2018.12.015.

[19] M. Morales, J.J. Roa, J. Tartaj, M. Segarra, A review of doped lanthanum gallates as electrolytes for intermediate temperature solid oxides fuel cells: From materials processing to electrical and thermo-mechanical properties. J. Eur. Ceram. Soc. 36 (2016) 1-16. https://doi.org/10.1016/j.jeurceramsoc.2015.09.025

[20] D. Marrero-López, J. Peña-Martínez, J.C. Ruiz-Morales, M.C. Martín-Sedeño, J.R. Ramos-Barrado, Microstructure and conductivity of $La_{1-x}Sr_xGa_{0.8}Mg_{0.2}O_{3-\delta}$ electrolytes prepared by freeze-drying method, J. Am. Ceram. Soc. 94 (2011) 1031-1039. https://doi.org/10.1111/j.1551-2916.2010.04233.x

[21] L. Shu, J. Sunarso, S.S. Hashim, J. Mao, W. Zhou, F. Liang Advanced perovskite anodes for solid oxide fuel cells: A review. Int. J. Hydrog. Energy 44 (2019) 31275-31304. https://doi.org/10.1016/j.ijhydene.2019.09.220

[22] M. Rafique, H. Nawaz, M.S. Rafique, M.B. Tahir, G. Nabi, N.R. Khalid, Material and method selection for efficient solid oxide fuel cell anode: Recent advancements and reviews. Int J. Energy Res. 43 (2019) 2423-2446. https://doi.org/10.1002/er.4210.

[23] S. Tao, J.T.S. Irvine, A redox-stable efficient anode for solid-oxide fuel cells. Nat. Mater. 2 (2003) 320-323. https://doi.org/10.1038/nmat871

[24] Q. Liu, X. Dong, G. Xiao, F. Zhao, F. Chen, A novel electrode material for symmetrical SOFCs. Adv. Mater. 22 (2010) 5478-5482. https://doi.org/10.1002/adma.201001044

[25] J.C. Ruíz-Morales, J. Canales-Vázquez, C. Savaniu, D. Marrero-López, W. Zhou, J.T.S. Irvine, Disruption of extended defects in solid oxide fuel cell anodes for methane oxidation. Nature 439 (2006) 568-571. https://doi.org/10.1038/nature04438

[26] S. Dwivedi, Solid oxide fuel cell: Materials for anode, cathode and electrolyte. Int. J. Hydrog. Energy 45 (2020) 23988-24013. https://doi.org/10.1016/j.ijhydene.2019.11.234.

[27] Z. Zakaria, Z.A. Mat, S.H.A. Hassan, Y.B. Kar, A review of solid oxide fuel cell component fabrication methods toward lowering temperature. Int. J. Energy Res. 44 (2020) 594-611. https://doi.org/10.1002/er.4907

[28] S.B. Adler, Factors governing oxygen reduction in solid oxide fuel cell cathodes. Chem. Rev. 104 (2004) 4791-4843. https://doi.org/10.1021/cr020724o

[29] G. Li, Y. Gou, J. Qiao, W. Sun, Z. Wang, K. Sun Recent progress of tubular solid oxide fuel cell: From materials to applications. J. Power Sources 477 (2020) 228693. https://doi.org/10.1016/j.jpowsour.2020.228693

[30] D. Panthi, N. Hedayat, T. Woodson, B.J. Emley, Y. Du, Tubular solid oxide fuel cells fabricated by a novel freeze casting method. J. Am. Ceram. Soc. 103 (2020) 878-888. https://doi.org/10.1111/jace.16781

[31] Y. Lyu, F. Wang, D. Wang, Z. Jin, Alternative preparation methods of thin films for solid oxide fuel cells: review. Mater Technol 5 (2020) 212-227. https://doi.org/10.1080/10667857.2019.1674478.

[32] J.C. Ruiz-Morales, D. Marrero-López, M. Gálvez-Sánchez, J. Canales-Vázquez, C. Savaniu, S.N. Savvin. Engineering of materials for solid oxide fuel cells and other energy and environmental applications. Energy Environ. Sci. 3 (2010) 1670-1681. https://doi.org/10.1039/C0EE00166J.

[33] G.Y. Cho, Y.H. Lee, S.W. Cha, Multi-component nano-composite electrode for SOFCs via thin film technique. Renew. Energy 65 (2014) 130-136. https://doi.org/10.1016/j.renene.2013.07.044

[34] J.C. Ruíz-Morales, A. Tarancón, J. Canales-Vázquez, J. Méndez-Ramos, l. Hernández-Afonso, P. Acosta-Nora, J.R. Marín Rueda R. Fernández-González, Three dimensional printing of components and functional devices for energy and environmental applications. Energy Environ. Sci. 10 (2017) 846-859. https://doi.org/10.1039/C6EE03526D

[35] Y. Du, N. Hedayat, D. Panthi, H. Ilkhani, B.J. Emley, T. Woodson, Freeze-casting for the fabrication of solid oxide fuel cells: A review. Materialia 1 (2018) 198-210. https://doi.org/10.1016/j.mtla.2018.07.005.

[36] J.S. Cronin, Y.C.K. Chen-Wiegart, J. Wang, S.A. Barnett, Three-dimensional reconstruction and analysis of an entire solid oxide fuel cell by full-field transmission X-ray microscopy. J. Power Sources 233 (2013) 174-179. https://doi.org/10.1016/j.jpowsour.2013.01.060

[37] D. Marrero-López, J.C. Ruíz-Morales, J. Peña-Martínez, J. Canales-Vázquez, P. Núñez, Preparation of thin layer materials with macroporous microstructure for SOFC applications. J. Solid State Chem. 181 (2008) 685-692. https://doi.org/10.1016/j.jssc.2008.01.008.

[38] D. Ding, X. Li, S.Y. Lai, K. Gerdes, M. Liu, Enhancing SOFC cathode performance by surface modification through infiltration. Energy Environ. Sci. 7 (2014) 552-575. https://doi.org/10.1039/C3EE42926A

[39] Y.G. Guo, J.S. Hu, L.J. Wan, Nanostructured Materials for Electrochemical Energy Conversion and Storage Devices. Adv. Mater. 20 (2008) 2878-2887. https://doi.org/10.1002/adma.200800627

[40] L. Fan, B. Zhu, P.-C. Su, C. He, Nanomaterials and technologies for low temperature solid oxide fuel cells: Recent advances, challenges and opportunities. Nano Energy 45 (2018) 148-176. https://doi.org/10.1016/j.nanoen.2017.12.044.

[41] B. Timurkutluk, T. Altan, S. Toros, O. Genc, S. Celik, H.G. Korkmaz, Engineering solid oxide fuel cell electrode microstructure by a micro-modeling tool based on estimation of TPB length. Int. J. Hydrog. Energy 46 (2021) 13298-13317. https://doi.org/10.1016/j.ijhydene.2021.01.165

[42] J. Chen, X. Wang, P. Boldrin, N.P. Brandon, A. Atkinson, Hierarchical dual-porosity nanoscale nickel cermet electrode with high performance and stability. Nanoscale 11 (2019) 17746-17758. https://doi.org/10.1039/C9NR06740J

[43] J. Dabrowa, A. Olszewska, A. Falkenstein, C. Schwab, M. Szymczak, M. Zajusz, M. Mozdizierz, A. Mikula, K. Zielinska, K. Berent, T. Czeppe, M. Martin, K. Swierczek, An innovative approach to design SOFC air electrode materials: high entropy $La_{1-x}Sr_x(Co,Cr,Fe,Mn,Ni)O_{3-\delta}$ (x = 0, 0.1, 0.2, 0.3) perovskites synthesized by the sol–gel method. J. Mater. Chem. A 8 (2020) 24455-24468. https://doi.org/10.1039/D0TA06356H

[44] D. Marrero-López, M.C. Martín-Sedeño, J.C. Ruiz-Morales, P. Núñez, J.R. Ramos-Barrado, Preparation and characterisation of $La_{10-x}Ge_{5.5}Al_{0.5}O_{26\pm\delta}$ apatites by freeze-drying precursor method, Materials Research Bulletin 45(2010) 409-415. https://doi.org/10.1016/j.materresbull.2009.12.017

[45] S.T. Aruna, L.S. Balaji, S. Sentil Kumar, B. Shri Prakash, Electrospinning in solid oxide fuel cells - A review. Renew. Sustain. Energy Rev. 67 (2017) 673-682. https://doi.org/10.1016/j.rser.2016.09.003

[46] A. Enrico, W. Zhang, M.L. Traulsen, E.M. Sala, P. Costamagna, P. Holtappels, $La_{0.6}Sr_{0.4}Co_{0.2}Fe_{0.8}O_{3-\delta}$ nanofiber cathode for intermediate-temperature solid oxide fuel cells by water-based sol-gel electrospinning: Synthesis and electrochemical behavior. J. Eur. Ceram. Soc. 38 (2018) 2677-2686. https://doi.org/10.1016/j.jeurceramsoc.2018.01.034

[47] A.R. Studart, U.T. Gonzenbach, E. Tervoort, L.J. Gauckler, Processing Routes to Macroporous Ceramics: A Review. J. Am. Ceram. Soc. 89 (2006) 1771-1789. https://doi.org/10.1111/j.1551-2916.2006.01044.x

[48] N. Hedayat, Y. Du, H. Ilkhani, Review on fabrication techniques for porous electrodes of solid oxide fuel cells by sacrificial template methods. Renew. Sustain. Energy Rev. 77 (2017) 1221-1239. https://doi.org/10.1016/j.rser.2017.03.095

[49] F.J.A. Loureiro, D.A. Macedo, R.M. Nascimento, M.R. Cesário, J.PF. Grilo, A.A. Yaremchenko, D.P. Fagg, Cathodic polarisation of composite LSCF-SDC IT-SOFC electrode synthesised by one-step microwave self-assisted combustion. J. Eur. Ceram. Soc. 39 (2019) 1846-1853. https://doi.org/10.1016/j.jeurceramsoc.2019.01.013

[50] S.Y. Lee, J. Yun, W.-P. Tai, Synthesis of Ni-doped $LaSrMnO_3$ nanopowders by hydrothermal method for SOFC interconnect applications. Adv. Powder Tech. 29 (2018) 2423-2428. https://doi.org/10.1016/j.apt.2018.06.021

[51] M. Zhi, G. Zhou, Z. Hong, J. Wang, R. Gemmen, K. Gerdes, A. Manivannan, D. Ma, N. Wu, Single crystalline $La_{0.5}Sr_{0.5}MnO_3$ microcubes as cathode of solid oxide fuel cell. Energy Environ. Sci. 4 (2011) 139-144. https://doi.org/10.1039/C0EE00300J

[52] Y. Namgung, J. Hong, A. Kumar, D.-K. Lim, S.-J. Song, One step infiltration induced multi-cation oxide nanocatalyst for load proof SOFC application. Appl. Catal. B Environ. 267 (2020) 118374. https://doi.org/10.1016/j.apcatb.2019.118374

[53] M. Zhi, N. Mariani, R. Gemmen, K. Gerdes, Nanofibers scaffold for cathode of solid oxide fuel cells. Energy Environ. Sci. 4 (2011) 417-420. https://doi.org/10.1039/C0EE00358A

[54] P.A. Connor, X. Yue, C.D. Savaniu, R. Price, G. Triantafyllou, M. Cassidy, G. Kerherve, D.J. Payne, R.C. Maher, L.F. Cohen, R.I. Tomov, B.A. Glowacki, R.V. Kumar, J.T.S. Irvine, Tailoring SOFC Electrode Microstructures for Improved Performance. Adv. Energy Mater. 8 (2018) 1800120. https://doi.org/10.1002/aenm.201800120

[55] J. Leng, Z. Wang, J. Wang, H.-H. Wu, G. Yan, X. Li, H. Guo, Y. Liu, Q. Zhang, Z. Guo, Advances in nanostructures fabricated *via* spray pyrolysis and their applications in energy storage and conversion. Chem. Soc. Rev. 48 (2019) 3015-3072. https://doi.org/10.1039/C8CS00904J

[56] D.S. Jung, Y.N. Ko, Y.C. Kang, S.B. Park, Recent progress in electrode materials produced by spray pyrolysis for next-generation lithium ion batteries. Adv. Powder Technol. 25 (2014) 18-31. https://doi.org/10.1016/j.apt.2014.01.012

[57] P.S. Patil, Versatility of chemical spray pyrolysis technique. Mater. Chem. Phys. 59 (1999) 185-198. https://doi.org/10.1016/S0254-0584(99)00049-8

[58] D. Perednis, L.J. Gauckler, Thin film deposition using spray pyrolysis. J. Electroceramics 14 (2005) 103-111. https://doi.org/10.1007/s10832-005-0870-x

[59] S.R. Ardekani, A.S.R. Aghdam, M. Nazari, A. Bayat, E. Yazdani, E. Saievar-Iranizad, A comprehensive review on ultrasonic spray pyrolysis technique: Mechanism, main parameters and applications in condensed matter, J. Anal. Appl. Pyrolysis 141 (2019) 104631. https://doi.org/10.1016/j.jaap.2019.104631

[60] R. Martínez-Bautista, S.M. Fernández-Valverde, A. Tejeda-Cruz, J.A. Chávez-Carvayar, Structural, morphological and electrical characterization of ceria-based nanostructured thin films obtained by ultrasonic spray pyrolysis. Bol. Soc. Esp. Ceram. V. 58 (2019) 38-47. https://doi.org/10.1016/j.bsecv.2018.06.004

[61] O. Wilhelm, S.E. Pratsinis, D. Perednis, L.J. Gauckler, Electrospray and pressurized spray deposition of yttria-stabilized zirconia films. Thin Solid Films 479 (2005) 121. https://doi.org/10.1016/j.tsf.2004.11.206

[62] A.M. Ganan-Calvo, J. Davila, A. Barrero, Current and droplet size in the electrospraying of liquids. Scaling laws. J. Aerosol Sci. 28 (1997) 249. https://doi.org/10.1016/S0021-8502(96)00433-8

[63] A. Jaworek, A.T. Sobczyk, Electrospraying route to nanotechnology: An overview, J. Electrost. 66 (2008) 197. https://doi.org/10.1016/j.elstat.2007.10.001

[64] A. Lintanf, A. Mantoux, E. Blanquet, E. Djurado, Elaboration of Ta_2O_5 Thin Films Using Electrostatic Spray Deposition for Microelectronic Applications. J. Phys. Chem. C 111 (2007) 5708. https://doi.org/10.1021/jp0676585

[65] R. Neagu, D. Perednis, A. Princivalle, E. Djurado, Zirconia coatings deposited by electrostatic spray deposition. Influence of the process parameters. Surf. Coat. Technol. 200 (2006) 6815. https://doi.org/10.1016/j.surfcoat.2005.10.014

[66] N. Bailly, S. Georges, E. Djurado, Elaboration and electrical characterization of electrosprayed YSZ thin films for intermediate temperature-solid oxide fuel cells (IT-SOFC). Solid State Ion. 222 (2012) 1-7. https://doi.org/10.1016/j.ssi.2012.06.020

[67] T. Nguyen, E. Djurado, Deposition and characterization of nanocrystalline tetragonal zirconia films using electrostatic spray deposition. Solid State Ionics 138 (2001) 191. https://doi.org/10.1016/S0167-2738(00)00795-5

[68] N.I. Karageorgakis, A. Heel, A. Bieberle-Hütter, J.L.M. Rupp, T. Graule, L.J. Gauckler, Flame spray deposition of $La_{0.6}Sr_{0.4}CoO_{3-d}$ thin films: Microstructural characterization, electrochemical performance and degradation, J. Power Sources 195 (2010) 8152-8161. https://doi.org/10.1016/j.jpowsour.2010.06.089

[69] D. Nunes, A. Pimentel, L. Santos, P. Barquinha, L. Pereira, E. Fortunato, R. Martins, Synthesis, design, and morphology of metal oxide nanostructures. Metal Oxide Nanostructures (2019) 21-57, https://doi.org/10.1016/B978-0-12-811512-1.00002-3.

[70] E.K. Athanassiou, R.N. Grass, W.J. Stark, Chemical aerosol engineering as a novel tool for material science: from oxides to salt and metal nanoparticles, Aerosol Sci. Technol. 44 (2010) 161-172. https://doi.org/10.1080/02786820903449665

[71] N.I. Karageorgakis, A. Heel, T. Graule, L.J. Gauckler, Flame spray deposition of nanocrystalline $Ce_{0.8}Gd_{0.2}O_{2-\delta}$ dense thin films: Deposition mechanism and microstructure characterization Solid State Ion. 192 (2011) 464-471. https://doi.org/10.1016/j.ssi.2010.04.030

[72] D. Perednis, L.J. Gauckler, Solid oxide fuel cells with electrolytes prepared via spray pyrolysis. Solid State Ion. 166 (2004) 229-239. https://doi.org/10.1016/j.ssi.2003.11.011

[73] B.C.H. Steele, A. Heinzel, Materials for fuel-cell technologies. Nature 414 (2001) 345-352. https://doi.org/10.1038/35104620

[74] J. Fleig, Solid oxide fuel cell cathodes: polarization mechanisms and modeling of the electrochemical performance. Annu. Rev. Mater. Res. 33 (2003) 361-382. https://doi.org/10.1146/annurev.matsci.33.022802.093258

[75] A. Hauch, R. Küngas, P. Blennow, A.B. Hansen, J.B. Hansen, B.V. Mathiesen, M.B. Mogensen, Recent advances in solid oxide cell technology for electrolysis. Science 370 (2020) 6118. https://doi.org/10.1126/science.aba6118.

[76] M.L. Liu, J. Winnick, Fundamental issues in modeling of mixed ionic-electronic conductors (MIECs). Solid State Ion. 118 (1999) 11-21. https://doi.org/10.1016/S0167-2738(98)00451-2

[77] S.B. Adler, J.A. Lane, B.C.H. Steele, Electrode Kinetics of Porous Mixed-Conducting Oxygen Electrodes. J. Electrochem. Soc. 143 (1996) 3554-3564. https://doi.org/10.1149/1.1837252

[78] F.S. Baumann, J. Maier, J. Fleig, The polarization resistance of mixed conducting SOFC cathodes: A comparative study using thin film model electrodes. Solid State Ion. 179 (2018) 1198-1204. https://doi.org/10.1016/j.ssi.2008.02.059

[79] J.A. Lane, S.J. Benson, D. Waller, J.A. Kilner, Oxygen transport in $La_{0.6}Sr_{0.4}Co_{0.2}Fe_{0.8}O_{3-\delta}$. Solid State Ion., 121 (1999) 201-208. https://doi.org/10.1016/S0167-2738(99)00014-4.

[80] D. Chen, Z. Shao, Surface exchange and bulk diffusion properties of $Ba_{0.5}Sr_{0.5}Co_{0.8}Fe_{0.2}O_{3-\delta}$ mixed conductor. Int. J. Hydrog. Energy 36 (2011) 6948-6956. https://doi.org/10.1016/j.ijhydene.2011.02.087.

[81] J.-H. Kim, A. Manthiram, Layered $LnBaCo_2O_{5+\delta}$ perovskite cathodes for solid oxide fuel cells: an overview and perspective. J. Mat. Chem. A 3 (2015) 24195-24210. https://doi.org/10.1039/C5TA06212H.

[82] A.J.A. Aziz, N.A. Baharuddin, M.R. Somalu, A. Muchtar, Review of composite cathodes for intermediate-temperature solid oxide fuel cell applications. Ceram. Int. 46 (2020) 23314-23325. https://doi.org/10.1016/j.ceramint.2020.06.176

[83] L. Fan, C. Wang, M. Chen, B. Zhu, Recent development of ceria-based (nano)composite materials for low temperature ceramic fuel cells and electrolyte-free fuel cells. J. Power Sources 234 (2013) 154-174. https://doi.org/10.1016/j.jpowsour.2013.01.138.

[84] J.T.S. Irvine, D. Neagu, M.C. Verbraeken, C. Chatzichristodoulou, C. Graves, M.B. Mogensen, Evolution of the electrochemical interface in high-temperature fuel cells and electrolysers. Nat. Energy 1 (2016) 15014. https://doi.org/10.1038/nenergy.2015.14.

[85] M.Z. Khan, R.-H. Song, M.T. Mehran, S.-B. Lee, T.-H. Lim, Controlling cation migration and inter-diffusion across cathode/interlayer/electrolyte interfaces of solid oxide fuel cells: A review. Ceram. Int. 47 (2021) 5839-5869. https://doi.org/10.1016/j.ceramint.2020.11.002

[86] S. He, Q. Zhang, G. Maurizio, L. Catellani, K. Chen, Q. Chang, M. Santarelli, S.P. Jiang In Situ Formation of $Er_{0.4}Bi_{1.6}O_3$ Protective Layer at Cobaltite Cathode/Y_2O_3–ZrO_2 Electrolyte Interface under Solid Oxide Fuel Cell Operation Conditions. ACS Appl. Mater. Interfaces 10 (2018) 40549–40559. https://doi.org/10.1021/acsami.8b14026.

[87] D. Neagu, G. Tsekouras, D.N. Miller, H. Ménard, J.T.S. Irvine, *In situ* growth of nanoparticles through control of non-stoichiometry. Nat. Chem. 5 (2013) 916-923. https://doi.org/10.1038/nchem.1773.

[88] J.G. Leem J.-H. Myung, A.B. Naden, O.S. Jeon, Y.G. Shul, J.T.S. Irvine Replacement of Ca by Ni in a Perovskite Titanate to Yield a Novel Perovskite Exsolution Architecture for Oxygen-Evolution Reactions. Adv. Energy Mat. 10 (2020) 1903693. https://doi.org/10.1002/aenm.201903693

[89] T. Cao, O. Kwon, R.J. Gorte, J.M. Vohs, Metal Exsolution to Enhance the Catalytic Activity of Electrodes in Solid Oxide Fuel Cells. Nanomaterials 10 (2020) 2445. https://doi.org/10.3390/nano10122445.

[90] Y. Gao, D. Chen, M. Saccoccio, Z. Lu, F. Ciucci, From material design to mechanism study: Nanoscale Ni exsolution on a highly active A-site deficient anode material for solid oxide fuel cells. Nano Energy 27 (2016) 499-508. https://doi.org/10.1016/j.nanoen.2016.07.013

[91] O. Ben Mya, L. dos Santos-Gómez, J.M. Porras-Vázquez, M. Omari, J.R. Ramos-Barrado, D. Marrero-López, $La_{1-x}Sr_xFe_{0.7}Ni_{0.3}O_{3-\delta}$ as both cathode and anode materials for Solid Oxide Fuel Cells. Int. J. Hydrog. Energy 42 (2017) 23160-23169. https://doi.org/10.1016/j.ijhydene.2017.07.150

[92] A. Princivalle, D. Perednis, R. Neagu, E. Djurado, Microstructural Investigations of Nanostructured La(Sr)MnO_{3-d} Films Deposited by Electrostatic Spray Deposition, Chem. Mater. 16 (2004) 3733-3739. https://doi.org/10.1021/cm049158z

[93] H.A. Hamedani, D. Klaus-Hermann, D. Li, H. Peydaye-Saheli, H. Garmestani, M. Khaleel, Fabrication of gradient porous LSM cathode by optimizing deposition parameters in ultrasonic spray pyrolysis. Mat. Sci. Eng. B 153 (2008) 1-9. https://doi.org/10.1016/j.mseb.2008.07.006

[94] J. Im, I. Park, D. Shin, Electrochemical properties of nanostructured lanthanum strontium manganite cathode fabricated by electrostatic spray deposition, Solid State Ion. 192 (2011) 448-452. https://doi.org/10.1016/j.ssi.2010.05.050

[95] D. Marrero-López, L. dos Santos-Gómez, J. Canales-Vázquez, F. Martín, J.R. Ramos-Barrado, Stability and performance of nanostructured $La_{0.8}Sr_{0.2}MnO_3$ cathodes deposited by spray-pyrolysis, Electrochim. Acta 134 (2014) 159-166. https://doi.org/10.1016/j.electacta.2014.04.154

[96] D. Marinha, C. Rossignol, E. Djurado, Influence of electrospraying parameters on the microstructure of $La_{0.6}Sr_{0.4}Co_{0.2}Fe_{0.8}O_{3-\delta}$ films for SOFCs, J. Solid State Chem. 182 (2009) 1742-1748. https://doi.org/10.1016/j.jssc.2009.04.018

[97] D. Marinha, L. Dessemond, J.S. Cronin, J.R. Wilson, S.A. Barnett, E. Djurado, Microstructural 3D Reconstruction and Performance Evaluation of LSCF Cathodes Obtained by Electrostatic Spray Deposition, Chem. Mater. 23 (2011) 5340-5348. https://doi.org/10.1021/cm2016998

[98] D. Marinha, J. Hayd, L. Dessemond, E. Ivers-Tiffée, E. Djurado, Performance of (La,Sr)(Co,Fe)O_{3-x} double-layer cathode films for intermediate temperature solid oxide fuel cell. J. Power Sources 196 (2011) 5084-5090. https://doi.org/10.1016/j.jpowsour.2011.01.063

[99] C. Sindiraç, S. Akkurt, Microstructural investigation of the effect of electrospraying parameters on LSCF films. Int. J. Hydrog. Energy 45 (2020) 35139-35148. https://doi.org/10.1016/j.ijhydene.2020.02.194

[100] D. Marrero-López, R. Romero, F. Martín, J.R. Ramos-Barrado, Effect of the deposition temperature on the electrochemical properties of $La_{0.6}Sr_{0.4}Co_{0.8}Fe_{0.2}O_{3-\delta}$ cathode prepared by conventional spray-pyrolysis, J. Power Sources 255 (2014) 308-317. https://doi.org/10.1016/j.jpowsour.2014.01.021

[101] B.S. Prakash, N. Balaji, S.S. Kumar, S.T. Aruna, Microstructure and Polarization Studies on Interlayer Free $La_{0.65}Sr_{0.3}Co_{0.2}Fe_{0.8}O_{3-d}$ Cathodes Fabricated on Yttria Stabilized Zirconia by Solution Precursor Plasma Spraying. Fuel cells 16 (2016) 617-627. https://doi.org/10.1002/fuce.201600119

[102] Y.-P. Wang, S.-H. Liu, H.-Y. Zhang, C.-X. Li, S.-L. Zhang, G.-J. Yang, C.-J. Li, Structured $La_{0.6}Sr_{0.4}Co_{0.2}Fe_{0.8}O_{3-\delta}$ cathode with large-scale vertical cracks by atmospheric laminar plasma spraying for IT-SOFCs. J. Alloys Compd. 825 (2020) 153865. https://doi.org/10.1016/j.jallcom.2020.153865

[103] J. Lee, I. Park, H. Lee, D. Shin, Effects of embossing structure on the performance of intermediate-temperature solid oxide fuel cells with gadolinium-doped ceria electrolyte. J. Power Sources 212 (2012) 35-42. https://doi.org/10.1016/j.jpowsour.2012.03.078

[104] T. Ryll, P. Reibisch, L. Schlagenhauf, A. Bieberle-Huetter, M. Döbeli, J.L.M. Rupp, L.J. Gauckler, Lanthanum nickelate thin films deposited by spray pyrolysis: Crystallization, microstructure and electrochemical properties. J. Eur. Ceram. Soc. 32 (2012) 1701-1709. https://doi.org/10.1016/j.jeurceramsoc.2011.12.032

[105] L. dos Santos-Gómez, J.M. Porras-Vázquez, J. Hurtado, E.R. Losilla, D. Marrero-López, Stability and electrochemical performance of nanostructured $La_2CuO_{4+\delta}$ cathodes. J. Alloys Compd. 788 (2019) 565-572 https://doi.org/10.1016/j.jallcom.2019.02.237

[106] R.A. Cox-Galhotra, S. McIntosh, Electrical conductivity relaxation of polycrystalline $PrBaCo_2O_{5+\delta}$ thin films. Solid State Ion. 228 (2012) 14-18. https://doi.org/10.1016/j.ssi.2012.09.001

[107] L. dos Santos-Gómez, J.M. Porras-Vázquez, E.R. Losilla, D. Marrero-López, Improving the efficiency of layered perovskite cathodes by microstructural optimization. J. Mater. Chem. A 5 (2017) 7896-7904. https://doi.org/10.1039/C6TA10946B

[108] S.-L. Zhang, K. Chen, A.-P. Zhang, C.-X. Li, C.-J. Li, Effect of Fe doping on the performance of suspension plasma-sprayed $PrBa_{0.5}Sr_{0.5}Co_{2-x}Fe_xO_{5+\delta}$ cathodes for intermediate-temperature solid oxide fuel cells. Ceram. Int. 43 (2017) 11648-11655. https://doi.org/10.1016/j.ceramint.2017.05.348

[109] U. Anjum, T.S. Khan, M. Agarwal, M.A. Haider, Identifying the Origin of the Limiting Process in a Double Perovskite $PrBa_{0.5}Sr_{0.5}Co_{1.5}Fe_{0.5}O_{5+\delta}$ Thin-Film Electrode for Solid Oxide Fuel Cells. ACS Appl. Mater. Interfaces 11 (2019) 25243-25253. https://doi.org/10.1021/acsami.9b06666

[110] L. dos Santos-Gómez, J. Zamudio-García, J.M. Porras-Vázquez, E.R. Losilla, D. Marrero-López, Nanostructured $BaCo_{0.4}Fe_{0.4}Zr_{0.1}Y_{0.1}O_{3-d}$ Cathodes with Different Microstructural Architectures, Nanomaterials 10 (2020) 1055. https://doi.org/10.3390/nano10061055

[111] H. Lv, Y.-J. Wu, B. Huang, B.-Y. Zhao, K. Hu, Structure and electrochemical properties of $Sm_{0.5}Sr_{0.5}Co_{1-x}Fe_xO_{3-\delta}$ cathodes for solid oxide fuel cells. Solid State Ion. 177 (2006) 901-906. https://doi.org/10.1016/j.ssi.2006.01.038

[112] E. Djurado, A. Salaün, G. Mignardi, A. Rolle, M. Burriel, S. Daviero-Minaud, R.N. Vannier, Electrostatic spray deposition of $Ca_3Co_4O_{9+\delta}$ layers to be used as cathode materials for IT-SOFC. Solid State Ion. 286 (2016) 102-110. https://doi.org/10.1016/j.ssi.2016.01.021

[113] E.O. Chi, Y.N. Kim, J.C. Kim, N.H. Hur, A macroporous perovskite manganite from colloidal templates with a curie temperaure of 320 K. Chem. Mater. 15 (2003) 1929-1931. https://doi.org/10.1021/cm034031f

[114] F. Tang, H. Fudouzi, T. Uchikoshi, Y. Sakka, Preparation of porous materials with controlled pore size and porosity. J. Eur. Ceram. Soc. 24 (2004) 341-344. https://doi.org/10.1016/S0955-2219(03)00223-1

[115] M. Sadakane, T. Asanuma, J. Kubo, W. Ueda, Facile procedure to prepare three-dimensionally ordered macroporous (3DOM) perovskite-type mixed metal oxides by colloidal crystal templating method. Chem. Mater. 17 (2005) 3546-3551. https://doi.org/10.1021/cm050551u

[116] J.C. Ruíz-Morales, J. Canales-Vázquez, J. Peña-Martínez, D. Marrero-López, J.T.S. Irvine, P. Núñez, Microstructural optimisation of materials for SOFC applications using PMMA microspheres. J. Mater. Chem. 16 (2006) 540-542. https://doi.org/10.1039/B515747A

[117] A. Arango-Díaz, J.A. Cecilia, L. dos Santos-Gómez, D. Marrero-López, E.R. Losilla, J. Jiménez-Jiménez, E. Rodríguez-Castellón, Characterization and performance in preferential oxidation of CO of CuO–CeO_2 catalysts synthesized using polymethyl metacrylate (PMMA) as template. Int. J. Hydrog. Energy 40 (2015) 11254-11260. https://doi.org/10.1016/j.ijhydene.2015.04.094

[118] Y. An, S.J. Skinner, D.W. McComb, Template-assisted fabrication of macroporous thin films for solid oxide fuel cells. J. Mater. Chem. 20 (2010) 248-254. https://doi.org/10.1039/B915882K

[119] E. Hernández, F. Baiutti, A. Morata, M. Torrell, A. Tarancón, Infiltrated mesoporous oxygen electrodes for high temperature co-electrolysis of H_2O and CO_2 in solid oxide electrolysis cells. J. Mater. Chem. A 6 (2018) 9699-9707. https://doi.org/10.1039/C8TA01045E

[120] L. Almar, B. Colldeforns, L. Yedra, S. Estradé, F. Peiró, A. Morata, T. Andreu, A. Tarancón, High-temperature long-term stable ordered mesoporous Ni–CGO as an anode for solid oxidefuel cells. J. Mat. Chem. A 1 (2013) 4531-4538. https://doi.org/10.1039/C3TA10439G

[121] L. Almar, A. Morata, M. Torrell, M. Gong, M. Liu, T. Andreu, A. Tarancón, Synthesis and characterization of robust, mesoporous electrodes for solid oxide fuel cells. J. Mater. Chem. A 4 (2016) 7650-7657. https://doi.org/10.1039/C6TA00321D.

[122] D. Beckel, U.P. Muecke, T. Gyger, G. Florey, A. Infortuna, L.J. Gauckler, Electrochemical performance of LSCF based thin film cathodes prepared by spray pyrolysis, Solid State Ionics 178 (2007) 407-415. https://doi.org/10.1016/j.ssi.2007.01.019

[123] L. dos Santos-Gómez, E.R. Losilla, F. Martín, J.R. Ramos-Barrado, D. Marrero-López, Novel Microstructural Strategies To Enhance the Electrochemical Performance of $La_{0.8}Sr_{0.2}MnO_{3-\delta}$ Cathodes, ACS Appl. Mater. Interfaces 7 (2015) 7197-7205. https://doi.org/10.1021/acsami.5b00255

[124] H. Shimada, T. Yamaguchi, H. Kishimoto, H. Sumi, Y. Yamaguchi, K. Nomura, Y. Fujishiro, Nanocomposite electrodes for high current density over 3 A cm^{-2} in solid oxide electrolysis cells. Nat. Commun. 10 (2019) 5432. https://doi.org/10.1038/s41467-019-13426-5

[125] H. Shimada, H. Sumi, Y. Yamaguchi, Y. Fujishiro, High-performance $Gd_{0.5}Sr_{0.5}CoO_{3-\delta}$ and $Ce_{0.8}Gd_{0.2}O_{1.9}$ nanocomposite cathode for achieving high power density in solid oxide fuel cells. Electrochim. Acta 368 (2021) 137869. https://doi.org/10.1016/j.electacta.2020.137679

[126] H. Shimada, Y. Fujimaki, Y. Fujishiro, Highly active and durable $La_{0.4}Sr_{0.6}MnO_{3-\delta}$ and $Ce_{0.8}Gd_{0.2}O_{1.9}$ nanocomposite electrode for high-temperature reversible solid oxide electrochemical cells. Ceram. Int. 46 (2020) 19617-19623. https://doi.org/10.1016/j.ceramint.2020.05.030

[127] A. Princivalle, E. Djurado, Nanostructured LSM/YSZ composite cathodes for IT-SOFC: A comprehensive microstructural study by electrostatic spray deposition. Solid State Ion. 179 (2008) 1921-1928. https://doi.org/10.1016/j.ssi.2008.05.006

[128] A. Princivalle, D. Perednis, R. Neagu, E. Djurado, Porosity Control of LSM/YSZ Cathode Coating Deposited by Electrospraying. Chem. Mater. 17 (2005) 1220-1227. https://doi.org/10.1021/cm048503h

[129] H. Shimada, T. Yamaguchi, H. Sumi, K. Nomura, Y. Yamaguchi, Y. Fujishiro, Extremely fine structured cathode for solid oxide fuel cells using Sr-doped $LaMnO_3$ and Y_2O_3-stabilized ZrO_2 nano-composite powder

synthesized by spray pyrolysis. J. Power Sources 341 (2017) 280-284. https://doi.org/10.1016/j.jpowsour.2016.12.002

[130] L. dos Santos-Gómez, J. Zamudio-García, J.M. Porras-Vázquez, E.R. Losilla, D. Marrero-López, Highly efficient $La_{0.8}Sr_{0.2}MnO_{3-\delta}$-$Ce_{0.9}Gd_{0.1}O_{1.95}$ nanocomposite cathodes for solid oxide fuel cells. Ceram. Int. 44 (2018) 4961-4966. https://doi.org/10.1016/j.ceramint.2017.12.089

[131] B.F. Angoua, P.R. Cantwell, E.A. Stach, E.B. Slamovich, Crystallization and electrochemical performance of $La_{0.6}Sr_{0.4}Co_{0.2}Fe_{0.8}O_{3-\delta}$-$Ce_{0.8}Gd_{0.2}O_{1.9}$ thin film cathodes processed by single solution spray pyrolysis. Solid State Ion. 203 (2011) 62-68. https://doi.org/10.1016/j.ssi.2011.08.017

[132] B.F. Angoua, E.B. Slamovich, Single solution spray pyrolysis of $La_{0.6}Sr_{0.4}Co_{0.2}Fe_{0.8}O_{3-\delta}$-$Ce_{0.8}Gd_{0.2}O_{1.9}$ (LSCF–CGO) thin film cathodes. Solid State Ion. 212 (2012) 10-17. https://doi.org/10.1016/j.ssi.2012.02.015

[133] J. Sar, O. Celikbilek, J. Villanova, L. Dessemond, C.L. Martin, E. Djurado, Three dimensional analysis of $Ce_{0.9}Gd_{0.1}O_{1.95}$–$La_{0.6}Sr_{0.4}Co_{0.2}Fe_{0.8}O_{3-d}$ oxygen electrode for solid oxide cells, J. Eur. Ceram. Soc. 35 (2015) 4497-4505. https://doi.org/10.1016/j.jeurceramsoc.2015.08.019

[134] J. Sar, L. Dessemond, E. Djurado, Electrochemical properties of graded and homogeneous $Ce_{0.9}Gd_{0.1}O_{2-d}$-$La_{0.6}Sr_{0.4}Co_{0.2}Fe_{0.8}O_{3-\delta}$ composite electrodes for intermediate-temperature solid oxide fuel cells. Int. J. Hydrog. Energy 41 (2016) 17037-17043. https://doi.org/10.1016/j.ijhydene.2016.07.236

[135] Ö. Celikbilek, D. Jauffres, L. Dessemond, M. Burriel, C.L. Martin, E. Djurado, A Coupled Experimental/Numerical Approach for Tuning High-Performing SOFC-Cathode. ECS Trans. 72 (2016) 81

[136] Ö. Celikbilek, D. Jauffres, E. Siebert, L. Dessemond, M. Burriel, C.L. Martin, E. Djurado, Rational design of hierarchically nanostructured electrodes for solid oxide fuel cells. J. Power Sources, 333 (2016) 72-82. https://doi.org/10.1016/j.jpowsour.2016.09.156.

[137] Ö. Çelikbilek, E. Siebert, D. Jauffrès, C.L. Martin, E. Djurado, Influence of sintering temperature on morphology and electrochemical performance of LSCF/GDC composite films as efficient cathode for SOFC. Electrochim. Acta 246 (2017) 1248-1258. https://doi.org/10.1016/j.electacta.2017.06.070

[138] L. dos Santos-Gómez, J.M. Porras-Vázquez, E.R. Losilla, F. Martín, J.R. Ramos-Barrado, D. Marrero-López, LSCF-CGO nanocomposite cathodes deposited in a single step by spray-pyrolysis, J. Eur. Ceram. Soc. 38 (2018) 1647-1653. https://doi.org/10.1016/j.jeurceramsoc.2017.10.010

[139] C. Sındıraç, A. Ahsen, O. Ozturk, S. Akkurt, V.I. Birss, A. Buyukaksoy, Fabrication of LSCF and LSCF-GDC nanocomposite thin films using polymeric precursors. Ionics 26 (2020) 913-925. https://doi.org/10.1007/s11581-019-03262-4

[140] H. Lee, I. Park, J. Park, G. Lee, D. Shin, Effects of dual porosity honeycomb structure in SSC–SDC composite cathode for SOFCs. Int. J. Hydrog. Energy 40 (2015) 11998-12002. https://doi.org/10.1016/j.ijhydene.2015.05.043

[141] J.-H. Kim, S.-S. Shin, H.-S. Noh, J.-W. Son, M. Choi, H. Kim, Tailoring ceramic membrane structures of solid oxide fuel cells via polymer-assisted electrospray deposition. J. Membrane Sci. 544 (2017) 234-242. https://doi.org/10.1016/j.memsci.2017.09.027

[142] R.K. Sharma, E. Djurado, Functionally graded and homogeneous composites of $La_2NiO_{4+\delta}$ and $La_{n+1}Ni_nO_{3n+1}$ (n = 2 and 3) solid oxide fuel cell cathodes, J. Mater. Chem. A 5 (2017) 22277-22287. https://doi.org/10.1039/C7TA06245A

[143] H. Lee, J. Choi, I. Park, D. Shin, Electrochemical performance of continuously gradient composite cathode fabricated by electro-static slurry spray deposition. Int. J. Hydrog. Energy 39 (2014) 14322-14327. https://doi.org/10.1016/j.ijhydene.2014.04.106

[144] H. Lee, S. Lee, T. Lee, S. Park, D. Shin, Long term stability of porosity gradient composite cathode controlled by electro-static slurry spray deposition. Int. J. Hydrog. Energy 42 (2017) 3748-3752. https://doi.org/10.1016/j.ijhydene.2016.09.077

[145] P. Holtappels, C. Bagger, Fabrication and performance of advanced multi-layer SOFC cathodes. J. Eur. Ceram. Soc. 22 (2002) 41-48. https://doi.org/10.1016/S0955-2219(01)00238-2

[146] L. dos Santos-Gómez, J.M. Porras-Vázquez, F. Martín, J.R. Ramos-Barrado, E.R. Losilla, D. Marrero-López, A novel multilaminated composite cathode for solid oxide fuel cells. Ceram. Int. 45 (2019) 18124-18127. https://doi.org/10.1016/j.ceramint.2019.05.296

[147] L. dos Santos-Gómez, J.M. Porras-Vázquez, F. Martín, J.R. Ramos-Barrado, E.R. Losilla, D. Marrero-López, Stability and performance of $La_{0.6}Sr_{0.4}Co_{0.2}Fe_{0.8}O_{3-\delta}$ nanostructured cathodes with $Ce_{0.8}Gd_{0.2}O_{1.9}$ surface coating. J. Power Sources 347 (2017) 178-185. https://doi.org/10.1016/j.jpowsour.2017.02.045

[148] M. Shah, S.A. Barnett, Solid oxide fuel cell cathodes by infiltration of $La_{0.6}Sr_{0.4}Co_{0.2}Fe_{0.8}O_{3-\delta}$ into Gd-Doped Ceria, Solid State Ion. 179 (2008) 2059-2064. https://doi.org/10.1016/j.ssi.2008.07.002

[149] Y. Li, W. Zhang, Y. Zheng, J. Chen, B. Yu, Y. Chen, M. Liu, Controlling cation segregation in perovskite-based electrodes for high electro-catalytic activity and durability. Chem. Soc. Rev. 46 (2017) 6345-6378. https://doi.org/10.1039/C7CS00120G

[150] J.M. Vohs, R.J. Gorte, High-performance SOFC cathodes prepared by infiltration. Adv. Mater. 21 (2009) 943-956. https://doi.org/10.1002/adma.200802428

[151] S.P. Jiang, Nanoscale and nano-structured electrodes of solid oxide fuel cells by infiltration: Advances and challenges. Int. J. Hydrog. Energy 37 (2012) 449-470. https://doi.org/10.1016/j.ijhydene.2011.09.067

[152] H. Tang, Z. Gong, Y. Wu, Z. Jin, W. Liu, Electrochemical performance of nanostructured LNF infiltrated onto LNO cathode for $BaZr_{0.1}Ce_{0.7}Y_{0.2}O_{3-d}$–based solid oxide fuel cell. Int. J. Hydrog. Energy 43 (2018) 19749-19756, doi:10.1016/j.ijhydene.2018.09.008

[153] S. Anelli, E. Hernández, L. Bernadet, X. Sun, A. Hagen, F. Baiutti, M. Torrell, A. Tarancón, Co-electrolysis of steam and carbon dioxide in large area solid oxide cells based on infiltrated mesoporous oxygen electrodes. J. Power Sources 478 (2020) 228774. https://doi.org/10.1016/j.jpowsour.2020.228774

[154] S.-L. Zhang, H. Wang, T. Yang, M.Y. Lu, C.-X. Li, C.-J. Li, S.A. Barnett, Advanced oxygen-electrode-supported solid oxide electrochemical cells with $Sr(Ti,Fe)O_{3-\delta}$-based fuel electrodes for electricity generation and hydrogen production. J. Mater. Chem. A 8 (2020) 25867-25879. https://doi.org/10.1039/D0TA06678H

[155] P. Qiu, X. Yang, L. Zou, T. Zhu, Z. Yuan, L. Jia, J. Li, F. Chen, $LaCrO_3$-Coated $La_{0.6}Sr_{0.4}Co_{0.2}Fe_{0.8}O_{3-\delta}$ Core–Shell Structured Cathode with Enhanced Cr Tolerance for Intermediate-Temperature Solid Oxide Fuel Cells. ACS Appl. Mater. Interfaces 12 (2020) 29133-29142. https://doi.org/10.1021/acsami.0c01962

[156] L. dos Santos-Gómez, J.M. Porras-Vázquez, F. Martín, J.R. Ramos-Barrado, E.R. Losilla, D. Marrero-López, An easy and innovative method based on spray-pyrolysis deposition to obtain high efficiency cathodes for Solid Oxide Fuel Cells. J. Power Sources 319 (2016) 48-55. https://doi.org/10.1016/j.jpowsour.2016.04.034

[157] R.K. Sharma, M. Burriel, L. Dessemond, J.M. Bassat, E. Djurado, Design of interfaces in efficient $Ln_2NiO_{4+\delta}$ (Ln = La, Pr) cathodes for SOFC applications. J. Mater. Chem. A 4 (2016) 12451-12462. https://doi.org/10.1039/C6TA04845E

[158] Y.-H. Song, S.U. Rehman, H.-S. Kim, H.-S. Song, R.-H. Song, T.-H.; Lim, J.-E. Hong, S.-J. Park, J.-Y. Huh, S.-B. Lee, Facile surface modification of LSCF/GDC cathodes by epitaxial deposition of $Sm_{0.5}Sr_{0.5}CoO_3$ via ultrasonic spray infiltration. J. Mater. Chem. A 8 (2020) 3967-3977. https://doi.org/10.1039/C9TA11704K

[159] T. Hong, S. Lee, P. Ohodnicki, K.A. Brinkman, A highly scalable spray coating technique for electrode infiltration: Barium carbonate infiltrated $La_{0.6}Sr_{0.4}Co_{0.2}Fe_{0.8}O_{3-\delta}$ perovskite structured electrocatalyst with

demonstrated long term durability. Int. J. Hydrog. Energy 42 (2017) 24978-24988. https://doi.org/10.1016/j.ijhydene.2017.08.091

[160] T. Hong, F. Chen, C. Xia, Barium carbonate nanoparticle as high temperature oxygen reduction catalyst for solid oxide fuel cell. Electrochem. Commun. 51 (2015) 93-97. https://doi.org/10.1016/j.elecom.2014.12.017

[161] S.P. Simner, M.D. Anderson, M.H. Engelhard, J.W. Stevenson, Degradation Mechanisms of La–Sr–Co–Fe–O_3 SOFC Cathodes. Electrochem. Solid State Lett. 9 (2006) A478-A481. https://doi.org/10.1149/1.2266160

[162] M.E. Lynch, L. Yang, W. Qin, J.J. Choi, M. Liu, K. Blinn, M. Liu. Enhancement of $La_{0.6}Sr_{0.4}Co_{0.2}Fe_{0.8}O_{3-\delta}$ durability and surface electrocatalytic activity by $La_{0.85}Sr_{0.15}MnO_{3\pm\delta}$ investigated using a new test electrode platform. Energy Environ. Sci. 4 (2011) 2249-2258. https://doi.org/10.1039/C1EE01188J

[163] Y. Gong, R.L. Patel, X. Liang, D. Palacio, X. Song, J.B. Goodenough, K. Huang, Atomic Layer Deposition Functionalized Composite SOFC Cathode $La_{0.6}Sr_{0.4}Fe_{0.8}Co_{0.2}O_{3-\delta}$-$Gd_{0.2}Ce_{0.8}O_{1.9}$: Enhanced Long-Term Stability. Chem. Mater 25 (2013) 4224-4231. https://doi.org/10.1021/cm402879r

[164] S. Molin, A. Chrzan, J. Karczewski, D. Szymczewska, P. Jasinski, THE ROLE OF THIN FUNCTIONAL LAYERS IN SOLID OXIDE FUEL CELLS. Electrochim. Acta 202 (2016) 136-145. https://doi.org/10.1016/j.electacta.2016.04.075

[165] R.K. Sharma, M. Burriel, L. Dessemond, V. Martin, J.-M. Bassat, E. Djurado, An innovative architectural design to enhance the electrochemical performance of La_2NiO_{4-d} cathodes for solid oxide fuel cell applications. J. Power Sources 316 (2016) 17-28. https://doi.org/10.1016/j.jpowsour.2016.03.067

[166] N.I. Khamidy, J. Laurencin, E. Djurado, Improving the electrochemical performance of $LaPrNiO_{4+\delta}$ as an oxygen electrode for intermediate temperature solid oxide cells by varying the architectural design. J. Electroanal. Chem. 849 (2019) 113373. https://doi.org/10.1016/j.jelechem.2019.113373

[167] N.I. Khamidy, J. Laurencin, D.F. Sanchez, F. Monaco, F. Charlot, E. Djurado, Durability of nanostructured $LaPrNiO_{4+\delta}$ electrode for solid oxide cells: Electrochemical, microstructural, and structural investigation. J. Power Sources 450 (2020) 227724. https://doi.org/10.1016/j.jpowsour.2020.227724

[168] R.K. Sharma, S.-K. Cheah, M. Burriel, L. Dessemond, J.-M. Bassat, E. Djurado, Design of $La_{2-x}Pr_xNiO_{4+\delta}$ SOFC cathodes: a compromise between electrochemical performance and thermodynamic stability. J. Mater. Chem. A 5 (2017) 1120-1132. https://doi.org/10.1039/C6TA08011A

[169] R.K. Sharma, E. Djurado, An efficient hierarchical nanostructured Pr_6O_{11} electrode for solid oxide fuel cells. J. Mater. Chem. A 6 (2018) 10787. https://doi.org/10.1039/C8TA00190A

[170] C. Nicollet, A. Flura, V. Vibhu, A. Rougier, J.-M. Bassat, J.-C. Grenier, An innovative efficient oxygen electrode for SOFC: Pr_6O_{11} infiltrated into Gd-doped ceria backbone. Int. J. Hydrog. Energy 41 (2016) 15538-15544. https://doi.org/10.1016/j.ijhydene.2016.04.024

[171] R.K. Sharma, N.I. Khamidy, L. Rapenne, F. Charlot, H. Moussaoui, J. Laurencin, E. Djurado, Highly efficient architectured Pr_6O_{11} oxygen electrode for solid oxide fuel cell. J. Power Sources 419 (2019) 171-180. https://doi.org/10.1016/j.jpowsour.2019.02.077

[172] J.D. Castro-Robles, N. Soltani, J.Á. Chávez-Carvayar, Structural, morphological and transport properties of nanostructured $La_{1-x}Sr_xCo_{0.2}Fe_{0.8}O_{3-\delta}$ thin films, deposited by ultrasonic spray pyrolysis. Mater. Chem. Phys. 225 (2019) 50-54. https://doi.org/10.1016/j.matchemphys.2018.12.053

[173] O. Celikbilek, C.-A. Thieu, F. Agnese, E. Calì, C. Lenser, N.H. Menzler, J.-W. Son, S.J. Skinner, E. Djurado, Enhanced catalytic activity of nanostructured, A-site deficient $(La_{0.7}Sr_{0.3})_{0.95}(Co_{0.2}Fe_{0.8})O_{3-d}$ for SOFC cathodes. J. Mater. Chem. A 7 (2019) 25102-25111. https://doi.org/10.1039/C9TA07697B

[174] S.S. Shin, J.H. Kim, G. Li, S.Y. Lee, J.-W. Son, H. Kim, M. Choi, A highly activated and integrated nanoscale interlayer of cathodes in low-temperature solid oxide fuel cells via precursor-solution electrospray method. Int. J. Hydrog. Energy 44 (2019) 4476-4483. https://doi.org/10.1016/j.ijhydene.2018.11.143

[175] S. Molin, P.Z. Jasinski, Improved performance of $LaNi_{0.6}Fe_{0.4}O_3$ solid oxide fuel cell cathode by application of a thin interface cathode functional layer. Mater. Lett. 189 (2017) 252-255. https://doi.org/10.1016/j.matlet.2016.11.101.

[176] J. Zamudio-García, N. Albarrán-Aroca, J.M. Porras-Vázquez, E.R. Losilla, D. Marrero-López, Influence of $Bi_{1.5}Y_{0.5}O_3$ Active Layer on the Performance of Nanostructured $La_{0.8}Sr_{0.2}MnO_3$ Cathode. Appl. Nano 1 (2020) 14-24. https://doi.org/10.3390/applnano1010003

[177] V. Zapata-Ramírez, L. dos Santos-Gómez, G.C. Mather, D. Marrero-López, D. Pérez-Coll, Enhanced Intermediate-Temperature Electrochemical Performance of Air Electrodes for Solid Oxide Cells with Spray-Pyrolyzed Active Layers. ACS Appl. Mater. Interfaces 12 (2020) 10571-10578. https://doi.org/10.1021/acsami.9b22966

[178] B. Kamecki, J. Karczewski, P. Jasiński, S. Molin, Improvement of Oxygen Electrode Performance of Intermediate Temperature Solid Oxide Cells by Spray Pyrolysis Deposited Active Layers. Adv. Mater. Interfaces 8 (2021) 2002227. https://doi.org/10.1002/admi.202002227

[179] L. Zhang, G. Chen, R. Dai, X. Lv, D. Yang, S. Geng, A review of the chemical compatibility between oxide electrodes and electrolytes in solid oxide fuel cells. J. Power Sources 492 (2021) 229630. https://doi.org/10.1016/j.jpowsour.2021.229630

[180] L. dos Santos-Gómez, J. Hurtado, J.M. Porras-Vázquez, E.R. Losilla, D. Marrero-López, Durability and performance of CGO barriers and LSCF cathode deposited by spray-pyrolysis. J. Eur. Ceram. Soc. 38 (2018) 3518-3526. https://doi.org/10.1016/j.jeurceramsoc.2018.03.024

[181] J.L.M. Rupp, L.J. Gauckler, Microstructures and electrical conductivity of nanocrystalline ceria-based thin films. Solid State Ion. 177 (2006) 2513-2518. https://doi.org/10.1016/j.ssi.2006.07.033

[182] B. Scherrer, J. Martynczuk, H. Galinski, J.G. Grolig, S. Binder, A. Bieberle-Hütter, J.L.M. Rupp, M. Prestat, L.J. Gauckler, Microstructures of YSZ and CGO Thin Films Deposited by Spray Pyrolysis: Influence of Processing Parameters on the Porosity. Adv. Funct. Mater. 22 (2012) 3509-3518. https://doi.org/10.1002/adfm.201200454

[183] L. dos Santos-Gómez, J. Zamudio-García, J.M. Porras-Vázquez, E.R. Losilla, D. Marrero-López, Highly oriented and fully dense CGO films prepared by spray-pyrolysis and different precursor salts. J. Eur. Ceram. Soc. 40 (2020) 3080-3088. https://doi.org/10.1016/j.jeurceramsoc.2020.03.026

[184] S. Molin, J. Karczewski, B. Kamecki, A. Mroziński, S.-F. Wang, P. Jasiński, Processing of $Ce_{0.8}Gd_{0.2}O_{2-\delta}$ barrier layers for solid oxide cells: The effect of preparation method and thickness on the interdiffusion and electrochemical performance. J. Eur. Ceram. Soc. 40 (2020) 5626-5633. https://doi.org/10.1016/j.jeurceramsoc.2020.06.006

[185] A.O. Stoermer, J.L.M. Rupp, L.J. Gauckler, Spray pyrolysis of electrolyte interlayers for vacuum plasma-sprayed SOFC. Solid State Ion. 177 (2006) 2075-2079. https://doi.org/10.1016/j.ssi.2006.06.033

[186] X. Ma, J. Dai, H.Zhang, J. Roth, T.D. Xiao, D.E. Reisner, Solid Oxide Fuel Cell Development by Using Novel Plasma Spray Techniques. J. Fuel Cell Sci. Technol. 2 (2005) 190-196. https://doi.org/10.1115/1.1928928

[187] L.-S. Wang, C.-X. Li, C.-J. Li, G.-J. Yang, Performance of $La_{0.8}Sr_{0.2}Ga_{0.8}Mg_{0.2}O_{3-d}$ based SOFCs with atmospheric plasma sprayed La-doped CeO_2 buffer layer. Electrochim. Acta 275 (2018) 208-217. https://doi.org/10.1016/j.electacta.2018.04.101

[188] N.I. Karageorgakis, A. Heel, J.L.M. Rupp, M.H. Aguirre, T. Graule, L.J. Gauckler, Properties of Flame Sprayed $Ce_{0.8}Gd_{0.2}O_{1.9-\delta}$ Electrolyte Thin Films. Adv. Funct. Mater. 21 (2011) 532-539. https://doi.org/10.1002/adfm.201001622

[189] C. Rossignol, B. Roman, G.D. Benetti, E. Djurado, Elaboration of thin and dense CGO films adherent to YSZ by electrostatic spray deposition for IT-SOFC applications. New J. Chem. 35 (2011) 716-723. https://doi.org/10.1039/C0NJ00570C

[190] G. Constantin, C. Rossignol, J.-P. Barnes, E. Djurado, Interface stability of thin, dense CGO film coating on YSZ for solid oxide fuel cells. Solid State Ion. 235 (2013) 36-41. https://doi.org/10.1016/j.ssi.2013.01.015

[191] I. Hwang, J. Jeong, K. Lim, J. Jung, Microstructural characterization of spray-dried NiO-8YSZ particles as plasma sprayable anode materials for metal-supported solid oxide fuel cell. Ceram. Int. 43 (2017) 7728-7735. https://doi.org/10.1016/j.ceramint.2017.03.077

[192] C.-H. Lim, K.-L. Lee, Characterization of core-shell structured Ni-GDC anode materials synthesized by ultrasonic spray pyrolysis for solid oxide fuel cells. Ceram. Int. 42 (2016) 13715-13722. https://doi.org/10.1016/j.ceramint.2016.05.170

[193] S. Hashigami, H. Yoshida, D. Ueno, M. Kawano, T. Inagaki, Improvement of the redox durability of Ni-gadolinia doped ceria anodes due to the use of the composite particles prepared by spray pyrolysis method. J. Power Sources 248 (2014) 190-195. https://doi.org/10.1016/j.jpowsour.2013.09.073

[194] L. Liu, G.-Y. Kim, A. Chandra, Fabrication of solid oxide fuel cell anode electrode by spray pyrolysis. J. Power Sources 195 (2010) 7046-7053. https://doi.org/10.1016/j.jpowsour.2010.04.083

[195] M. Kawano, H. Yoshida, K. Hashino, H. Ijichi, S. Suda, K. Kawahara, T. Inagaki, Synthesis of matrix-type NiO–SDC composite particles by spray pyrolysis with acid addition for development of SOFC cermet anode. J. Power Sources 173 (2007) 45-52. https://doi.org/10.1016/j.jpowsour.2007.08.021

[196] C.-X. Li, C.-J. Li, L.-J. Guo, Effect of composition of NiO/YSZ anode on the polarization characteristics of SOFC fabricated by atmospheric plasma spraying. Int. J. Hydrog. Energy 35 (2010) 2964-2969. https://doi.org/10.1016/j.ijhydene.2009.05.041

[197] C. Metcalfe, E. Lay-Grindler, O. Kesler, Characterization of Ni–YSZ anodes for solid oxide fuel cells fabricated by solution precursor plasma spraying with axial feedstock injection. J. Power Sources 247 (2014) 831-839. https://doi.org/10.1016/j.jpowsour.2013.09.035

[198] M. Gupta, A. Weber, N. Markocsan, N. Heiden, Development of plasma sprayed Ni/YSZ anodes for metal supported solid oxide fuel cells. Surf. Coat. Technol. 318 (2017) 178-189. https://doi.org/10.1016/j.surfcoat.2016.09.014

[199] R. Nishida, K. Kakinuma, H. Nishino, T. Kamino, H. Yamashita, M. Watanabe, H. Uchida, Synthesis of nickel nanoparticles supported on hollow samaria-doped ceria particles via the solution-spray plasma technique: Anode catalysts for SOFCs. Solid State Ion. 180 (2009) 968-972. https://doi.org/10.1016/j.ssi.2009.04.005

[200] R. Nishida, P. Puengjinda, H. Nishino, K. Kaninuma, M.E. Brito, M. Watanabe, H. Uchida, High-performance electrodes for reversible solid oxide fuel cell/solid oxide electrolysis cell: Ni–Co dispersed ceria hydrogen electrodes. RSC Adv. 4 (2014) 16260. https://doi.org/10.1039/C3RA47089J

[201] L. Liu, G.Y. Kim, A. Chandra, A. Fabrication of solid oxide fuel cell anode electrode by spray pyrolysis. J. Power Sources 195 (2010) 7046-7053. https://doi.org/10.1016/j.jpowsour.2010.04.083

[202] P. Bohac, L. Gauckler, Chemical spray deposition of YSZ and GCO solid electrolyte films. Solid State Ion. 119 (1999) 317-312. https://doi.org/10.1016/S0167-2738(98)00521-9

[203] L. Liu, G.-Y. Kim, A.C. Hillier, A. Chandra, Microstructural and electrochemical impedance study of nickel–$Ce_{0.9}Gd_{0.1}O_{1.95}$ anodes for solid oxide fuel cells fabricated by ultrasonic spray pyrolysis. J. Power Sources 196 (2011) 3026-3032. https://doi.org/10.1016/j.jpowsour.2010.11.117

[204] L. Liu, G.-Y. Kim, A. Chandra, Modeling of Ni–CGO anode in a solid oxide fuel cell deposited by spray pyrolysis. J. Power Sources 210 (2012) 129-137. https://doi.org/10.1016/j.jpowsour.2012.03.031

[205] I. Taniguchi, T. Hosokawa, Deposition of SDC and NiO-SDC thin films and their surface morphology control by electrostatic spray deposition. J. Alloys Compd. 460 (2008) 464-471. https://doi.org/10.1016/j.jallcom.2007.05.093

[206] S. Jang, I. Hwang, J. Im, I. Park, D.W. Shin, Fabrication of nickel oxide-yttria stabilized zirconia films by electrostatic spray deposition. J. Ceram. Process. Res. 10 (2009) 798-802.

[207] B.-H. Hwang, C.-L. Chang, C.-S. Hsu, C.-Y. Fu, Electrostatic spray deposition of NiO/CGO films. J. Phys. D: Appl. Phys. 40 (2007) 3448. https://doi.org/10.1088/0022-3727/40/11/028

[208] S.-L. Zhang, C.-X. Li, C.-J. Li, Chemical compatibility and properties of suspension plasma-sprayed $SrTiO_3$-based anodes for intermediate-temperature solid oxide fuel cells. J. Power Sources 264 (2014) 195-205. https://doi.org/10.1016/j.jpowsour.2014.04.094

[209] K. Genji, K. Myoujin, T. Kodera, T. Ogihara, Synthesis and Electrical Properties of La Doped $SrTiO_3$ Powders by Ultrasonic Spray Pyrolysis. KEM 582 (2013) 115-118. https://doi.org/10.4028/www.scientific.net/KEM.582.115

[210] Y. Xie, R. Neagu, C.-S. Hsu, X. Zhang, C. Decès-Petit, Spray Pyrolysis Deposition of Electrolyte and Anode for Metal-Supported Solid Oxide Fuel Cell. J. Electrochem. Soc. 155 (2008) B407-B410. https://doi.org/10.1149/1.2840468

[211] R. Hui, J.O. Berghaus, C. Decès-Petit, W. Qu, S. Yick, J.G. Legoux, C. Moreau, High performance metal-supported solid oxide fuel cells fabricated by thermal spray. J. Power Sources 191 (2009) 371-376. https://doi.org/10.1016/j.jpowsour.2009.02.067

[212] D. Marcano, G. Mauer, R. Vaßen, A. Weber, Manufacturing of high performance solid oxide fuel cells (SOFCs) with atmospheric plasma spraying (APS) and plasma spray-physical vapor deposition (PS-PVD). Surf. Coat. Technol. 318 (2017) 170-177. https://doi.org/10.1016/j.surfcoat.2016.10.088

[213] Y.B. Matus, L.C. De Joghe, C.P. Jacobson, S.J. Visco, Metal-supported solid oxide fuel cell membranes for rapid thermal cycling. Solid State Ion. 176 (2005) 443-449. https://doi.org/10.1016/j.ssi.2004.09.056

[214] L. dos Santos-Gómez, J.M. Porras-Vázquez, E.R. Losilla, D. Marrero-López, Ti-doped $SrFeO_3$ nanostructured electrodes for symmetric solid oxide fuel cells. RSC Adv. 5 (2015) 107889. https://doi.org/10.1039/C5RA23771H